

Cosmic τ ensions Indirectly Correlate with Reionization Optical Depth

Itamar J. Allali,^a Lingfeng Li,^{a,b} Praniti Singh,^a JiJi Fan^{a,c}

^aDepartment of Physics, Brown University, Providence, RI 02912, USA

^bInternational Center of Theoretical Physics-Asia Pacific, Beijing 100190, China

^cBrown Theoretical Physics Center, Brown University, Providence, RI 02912, USA

E-mail: itamar_allali@brown.edu, praniti_singh@brown.edu, jiji_fan@brown.edu, l.f.li165@gmail.com

Abstract. The reionization optical depth τ_{reio} has interesting connections to existing cosmological anomalies. As first studied in the context of the Hubble tension in our previous paper, a larger τ_{reio} , which could be achieved by removing the Planck low- ℓ polarization data, could boost H_0 slightly, resulting in a mild reduction of the tension between the early- and late-universe determinations of H_0 . It has been shown later that a larger τ_{reio} could also relieve other anomalies including: the tension between BAO and CMB data, the neutrino mass tension, and the latest DESI plus supernovae data's tension with the standard cosmological constant scenario. In this paper, we systematically analyze the correlations between τ_{reio} and relevant cosmological parameters in the existing cosmic observation anomalies. In addition to Pearson correlation coefficients extracted directly from the covariance matrix, we also study partial correlation coefficients which measure intrinsic relationships between pairs of parameters removing the influence of other parameters. We show that τ_{reio} has weak intrinsic correlations with the parameters responsible for the tensions and anomalies discussed. The large direct Pearson correlations that allow larger τ_{reio} inferences to alleviate the cosmological tensions each arise from complicated networks through multiple parameters. As a result, the relationships between τ_{reio} and each anomaly are not independent of each other. We also employ our method of computing correlations to clarify the impact of large scale polarization data, and comment also on the effects of CMB observations from ACT and SPT.

Contents

1	Introduction	1
2	Methodology and Datasets	3
2.1	Evaluating Correlations	4
3	Correlations of τ_{reio} and Cosmic Tensions	5
3.1	Hubble Tension	7
3.2	BAO-CMB Tension	8
3.3	Neutrino Mass Tension	10
3.4	Nature of Dark Energy	13
4	Effects of Datasets	15
5	Conclusion	19
A	Correlations for CMB-PAS(EE)	24
B	Neutrino Mass with SN_{DES}	26
C	Correlations for SN_{DES} and $\text{SN}_{\text{Union3}}$ in $w_0 w_a \text{CDM}$	26
D	Posteriors for CMB-PAS	29

1 Introduction

The Λ CDM model is the most widely accepted cosmological model, compatible with a variety of observations spanning many epochs of cosmic history. Within this six-parameter framework, one such parameter is the reionization optical depth, τ_{reio} . The era of reionization marks a key phase in cosmic history, signaling the end of the “dark ages,” when the universe was mostly filled with neutral gas, and the beginning of star and galaxy formation accompanied by the reionization of baryonic matter.

Currently, τ_{reio} , is constrained through two different observations: measurement of the Cosmic Microwave Background (CMB) and astrophysical observations of early luminous galaxies. The CMB provides a probe of τ_{reio} by measuring CMB photons scattered by free electrons produced during reionization. This scattering suppresses the temperature anisotropy power spectrum at small angular scales and enhances the large-scale E-mode polarization signal, allowing precise constraints on τ_{reio} (see [1] for further details). On the other hand, the astrophysical approach [2, 3] indirectly infers τ_{reio} by studying the population of high redshift luminous galaxies, their production rate of ionizing photons, and the fraction of these photons that escape into the intergalactic medium to ionize neutral hydrogen. Although the *Planck* satellite CMB measurements currently give $\tau_{\text{reio}} = 0.0544 \pm 0.0073$ [4], recent astrophysical studies (or galaxy surveys) from the James Webb Space Telescope (JWST) [5, 6] suggest a higher value, potentially $\tau_{\text{reio}} \geq 0.07$ [7], mainly driven by a higher

photon production rate at early times [8, 9] and, sub-dominantly, the observation of more star-forming galaxies at high redshift [10, 11]. Moreover, several recent low-redshift surveys [12] suggest a higher photon escape fraction, which, when extrapolated to higher redshifts, implies an even greater value of $\tau_{\text{reio}} \sim 0.096$.

The JWST studies are potentially subject to substantial astrophysical uncertainties from observational bias in galaxy surveys, parameter extrapolation, and baryon physics modeling (see also [13–16]). Meanwhile, the precise constraints on τ_{reio} using CMB data is mainly driven by large-scale (low- ℓ) E-mode polarization data which are subject to largest uncertainties among all the CMB measurements. Interestingly, Ref. [17] has shown that the exclusion of large-scale CMB data pushes the value of τ_{reio} to a higher value, in the range preferred by the JWST studies.

While these new observations potentially challenge our current understanding of reionization, it is crucial to explore their impact on existing cosmological tensions/anomalies. In this work, we will focus on:

- **The Hubble tension:** This refers to the discrepancy in the value of the current expansion rate, H_0 , inferred from CMB measurements versus more direct observations of supernovae-based distance ladder methods [18–25].
- **The BAO-CMB tension:** There is a mild discrepancy between CMB datasets and the recent baryon acoustic oscillations (BAO) observations from the Dark Energy Spectroscopic Instrument (DESI) [26] in the most directly inferred parameters from BAO: the matter density, Ω_m and hr_d , with $h = H_0/(100 \text{ km/s/Mpc})$ and r_d the physical size of the sound horizon at the baryon drag epoch.
- **Neutrino mass:** There is a notable tension regarding the sum of neutrino masses $\sum m_\nu$ inferred from cosmological measurements and the lower bound imposed by neutrino oscillation experiments ($\sum m_\nu \geq 0.06 \text{ eV}$ for normal ordering and 0.1 eV for inverted hierarchy [27]). Within the ΛCDM framework, recent BAO measurements from DESI, when combined with the Planck CMB data, yield a posterior for $\sum m_\nu$ peaking near zero (for prior $\sum m_\nu \geq 0$), giving rise to an upper bound of $\sum m_\nu < 0.0642 \text{ eV}$ (95% C.L.)[28] and seeming to rule out inverted ordering.¹
- **Dynamical Dark Energy:** Recent BAO measurements from DESI, combined with CMB data (and various supernovae datasets), show a $\sim 2 - 4\sigma$ preference for dynamical dark energy (DE) over the standard ΛCDM model, when employing the Chevallier-Polarski-Linder (CPL) parameterization [32, 33] of the DE equation of state: $w(a) = w_0 + w_a(1 - a)$, which we refer to as the $w_0w_a\text{CDM}$ [26] model.

Recent studies have explored the impact of τ_{reio} measurements on these existing cosmological tensions. For instance, in our previous paper [34], it was first pointed out that increasing τ_{reio} by excluding low- ℓ EE CMB data can mildly alleviate the Hubble tension. Similarly, Ref. [35, 36] showed that raising τ_{reio} to around 0.09 relaxes the constraint on neutrino mass and reduces the preference for evolving DE. Additionally, Ref. [36] suggested that the BAO-CMB tension can also be mitigated by an increase in τ_{reio} . Other studies in the literature have recently focused on probing the epoch of reionization, see [37–40].

¹It has been shown that the data even favor unphysical negative extrapolations for the neutrino mass sum, see e.g. [28–31].

Motivated by these findings, in this work we investigate the correlations between τ_{reio} and other cosmological parameters within the context of the tensions described above. Specifically, we study both the Pearson correlation coefficients between parameters of interest, as well as partial correlation coefficients which take into account the effects of other parameters. We employ these measures of correlation to glean information about the relationship between τ_{reio} and each tension/anomaly. We begin in Section 2 by describing the datasets and methodology used in this work. In Section 3, we systematically present the correlations of τ_{reio} with other parameters within the context of all four tensions studied, using CMB data from *Planck*, BAO from DESI, and supernovae measurements from Pantheon+. In Section 4, we examine the effects of including or excluding different combinations of datasets, including CMB data from Atacama Cosmology Telescope (ACT) and the South Pole Telescope (SPT), as well as other supernovae datasets. Finally, we give concluding remarks in Section 5.

2 Methodology and Datasets

We conduct Markov Chain Monte Carlo (MCMC) simulations to explore the parameter space of several cosmological models and assess the correlations between parameters of interest. In particular, we will assess both the Pearson correlations and the partial (intrinsic) correlations between sets of parameters, as discussed further below, in the context of several combinations of datasets. We consider the following CMB observations:

- **CMB-P:** CMB observations from the *Planck* satellite, including: the Public Release 3 (PR3) `Commander` likelihood for the low- ℓ ($\ell < 30$) TT power spectrum [41]; the PR3 `SimA11` likelihood for the low- ℓ polarization EE spectrum [41]; the PR4 `Camspec` likelihood for high- ℓ TT, TE, and EE spectra ($30 < \ell < 2500$ TT, $30 < \ell < 2000$ TE, EE) [42–44]; and the combined *Planck* PR4 [45] and ACT Data Release 6 (DR6) [46, 47] lensing likelihood.
- **CMB-PA:** The same as **CMB-P**, with the *Planck* high- ℓ data restricted to TT $\ell \in [30, 1800]$, TE $\ell \in [30, 750]$, EE $\ell \in [30, 750]$; and the addition of the ACT DR6 multi-frequency likelihood `MFLike` [48] for high- ℓ TT $\ell \in [1800, 8500]$, TE $\ell \in [750, 8500]$, EE $\ell \in [750, 8500]$.
- **CMB-PS:** The same as **CMB-P**, with the *Planck* high- ℓ data restricted to TT $\ell \in [30, 2000]$, TE $\ell \in [30, 1200]$, EE $\ell \in [30, 1200]$; and the addition of the SPT-3G D1 likelihood `cand1` [49] for high- ℓ TT $\ell \in [1200, 3000]$, TE $\ell \in [1200, 4000]$, EE $\ell \in [1200, 4000]$.²
- **CMB-PAS:** The same as **CMB-P**, with the *Planck* high- ℓ data restricted to TT $\ell \in [30, 1800]$, TE $\ell \in [30, 750]$, EE $\ell \in [30, 750]$; the addition of the ACT DR6 multi-frequency likelihood `MFLike` [48] for high- ℓ TT $\ell \in [1800, 8500]$, TE $\ell \in [750, 8500]$, EE $\ell \in [750, 8500]$; and the SPT-3G D1 likelihood `cand1` [49] for high- ℓ TT $\ell \in [1200, 3000]$, TE $\ell \in [1200, 4000]$, EE $\ell \in [1200, 4000]$.³

²In the combinations **CMB-PS** and **CMB-PAS**, there is some overlap between the SPT and *Planck* data in the TT channel for our choices of ℓ ; since the sky fraction of SPT is small, we can approximate these observations to be uncorrelated as done in [49].

³In the combination **CMB-PAS**, there is also an overlap between ACT and SPT data, which again can be taken to be uncorrelated as done in [49], since the sky fraction overlap between the two experiments is small.

- **{CMB-P(EE), CMB-PA(EE), CMB-PS(EE), CMB-PAS(EE)}**: The same as the four datasets above with the removal of the low- ℓ EE *Planck* data from the `SimAll` likelihood.

When combining multiple CMB datasets, we have chosen the ranges of ℓ for each experiment such that *Planck* is chosen where it achieves higher precision, and SPT/ACT are chosen when their precision exceeds *Planck*, according to the comparison's made in [48, 49]. In addition to CMB data, we include the following BAO and supernovae (SN) data:

- **B**: BAO measurements from the DESI data release 2 (DR2) for effective redshifts $z = 0.295, 0.51, 0.706, 0.934, 1.321, 1.484, 2.33$ [26].
- **SN**: Type Ia supernovae catalog from Pantheon+ [50].
- **SN_{DES}**: Type Ia supernovae catalog for the Dark Energy Survey (DES) 5-year dataset [51].
- **SN_{Union3}**: Type Ia supernovae catalog from the Union3 compilation [52].

When not focusing on results that rely heavily on the choice of supernovae dataset, we will include the Pantheon+ set as default. Thus, the baseline dataset for this work will be the combination **CMB-P+B+SN** and the corresponding one without low- ℓ EE *Planck* data, **CMB-P(EE)+B+SN**.

We employ the Boltzmann-solver `CLASS` [53, 54] for computing the cosmic evolution for each point in parameter space, sampled by the `Cobaya` sampler [55, 56]. We use `getdist` for analyzing the samples [57].

2.1 Evaluating Correlations

We will assess correlations between parameters using the results of the MCMC analyses. First, the covariance matrix Σ_{ij} of a subset of parameters can be obtained straightforwardly from the MCMC samples. The diagonal components Σ_{ii} correspond to the variance of the i^{th} parameter, and the off-diagonal Σ_{ij} correspond to the covariance between the i^{th} and j^{th} parameters. Thus, the correlation between two parameters can be computed as follows:

$$R_{ij} = \frac{\Sigma_{ij}}{\sqrt{\Sigma_{ii}\Sigma_{jj}}} = \frac{\sigma_{ij}^2}{\sqrt{\sigma_i^2\sigma_j^2}}, \quad (2.1)$$

where R_{ij} is the Pearson correlation coefficient between the i^{th} and j^{th} parameters, corresponding to the correlation between the sets of these two parameters contained in the MCMC sample, under the assumption that these parameters are independent of other parameters. This is equivalent to the ratio of the covariance between the two parameters σ_{ij}^2 to the square root of the product of their respective variances σ_i^2 and σ_j^2 . Equivalently, the correlation matrix \mathbf{R} can be obtained as

$$\mathbf{R} = (\mathbf{\Sigma}_{\sqrt{\text{diag}}})^{-1} \times \mathbf{\Sigma} \times (\mathbf{\Sigma}_{\sqrt{\text{diag}}})^{-1}, \quad (2.2)$$

with $\mathbf{\Sigma}$ the covariance matrix, and $\mathbf{\Sigma}_{\sqrt{\text{diag}}}$ is a diagonal matrix containing the standard deviations of each parameter, or equivalently the square roots of the diagonal components of the covariance matrix.

We wish also to assess the intrinsic relationship between parameters, where the variation in other parameters is taken into account and effectively removed. Known as *partial correlations*, these measures are an indication of the correlation between a pair of parameters while factoring out the influence of any other correlated parameters. For instance, in the case of three correlated random parameters X , Y and Z , the partial correlation between X and Y is calculated by removing their correlation coefficient with Z :

$$\rho_{XY \cdot Z} = \frac{R_{XY} - R_{XZ}R_{ZY}}{\sqrt{1 - R_{XZ}^2}\sqrt{1 - R_{YZ}^2}}, \quad (2.3)$$

where R_{ij} is the Pearson correlation defined in Eq. (2.2). In a sample that is sufficiently Gaussian, the partial correlation between parameter X and Y can be considered as the Pearson correlation between them when all other parameters are fixed to their best-fit values. The approach is close to Figure 1 of [34] by doing fits with only two parameters.

Obtaining the partial correlations for multiple parameters is straightforward, similar to the Pearson correlations but working instead with the inverse of the covariance matrix, also known as the precision matrix, $\Omega \equiv \Sigma^{-1}$. The matrix of partial correlations ρ is given by

$$\rho = -(\Omega_{\sqrt{\text{diag}}})^{-1} \times \Omega \times (\Omega_{\sqrt{\text{diag}}})^{-1}, \quad (2.4)$$

where similarly $\Omega_{\sqrt{\text{diag}}}$ is a diagonal matrix containing the square roots of the diagonal elements of Ω .⁴ In practice, one can also only remove a subset of remaining parameters by considering a submatrix of the covariance matrix with irrelevant parameters excluded. In this work, we always ignore the nuisance parameters when calculating partial correlations, as they behave as noise to cosmological parameters. Note that the relation of Eq. (2.2) and (2.4) are dual to each other since $\Sigma = \Omega^{-1}$. In other words, one could also start with the partial correlation ρ and obtain the Pearson correlation R . In this sense, the Pearson correlation R and partial correlation ρ are dual descriptions of the data, with the latter discussed less often in cosmology.

3 Correlations of τ_{reio} and Cosmic Tensions

In this section, we will discuss the impact of τ_{reio} on existing cosmological anomalies, listed in Section 1, one by one. To demonstrate the effects of increasing τ_{reio} , we will compare MC samples obtained using CMB data with and without the low- ℓ EE data, as the removal of this data results in a larger value of τ_{reio} . To avoid clumsiness, we will present results mainly using the simplest CMB dataset **CMB-P(EE)** or **CMB-P**, plus **B** and **SN**. We will discuss the effects of adding ACT and SPT datasets in Section 4, as they will not modify the main conclusions. Additional results for correlations in the data combination **CMB-PAS** are given in Section A, and results involving **SN_{DES}** and **SN_{Union3}** are presented in Section C. Also, though we do not focus on presenting constraints for cosmological parameters in this work, we do provide posterior statistics and plots for the novel combination of CMB data presented in this work, **CMB-PAS**, in Section D.

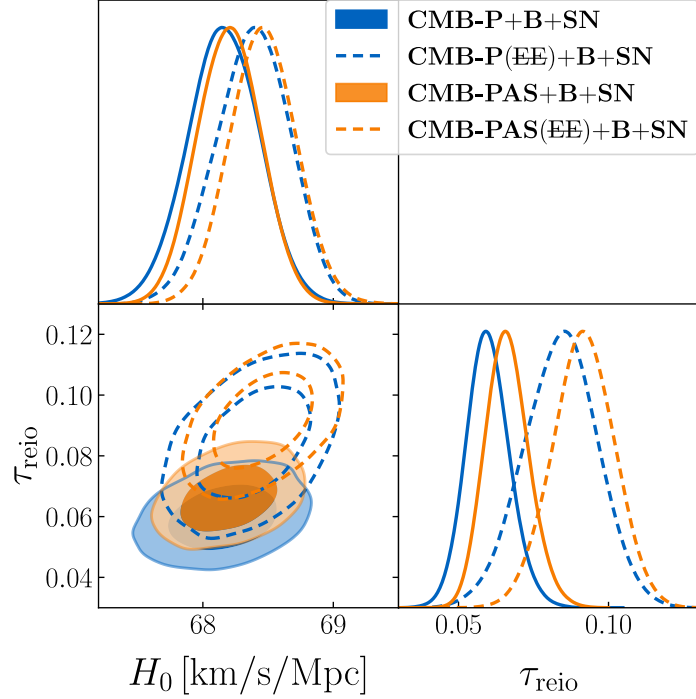


Figure 1: The one- and two-dimensional posterior distributions of H_0 and τ_{reio} in a series of fits to four different combinations of datasets, assuming ΛCDM .

Pearson	$\log(10^{10}A_s)$	n_s	H_0	ω_b	ω_{cdm}	τ_{reio}
$\log(10^{10}A_s)$	1.00	0.30	0.43	0.23	-0.41	0.98
n_s	0.30	1.00	0.49	0.23	-0.48	0.33
H_0	0.43	0.49	1.00	0.59	-0.89	0.43
ω_b	0.23	0.23	0.59	1.00	-0.25	0.22
ω_{cdm}	-0.41	-0.48	-0.89	-0.25	1.00	-0.43
τ_{reio}	0.98	0.33	0.43	0.22	-0.43	1.00

Partial	$\log(10^{10}A_s)$	n_s	H_0	ω_b	ω_{cdm}	τ_{reio}
$\log(10^{10}A_s)$	—	-0.13	0.09	0.00	0.10	0.98
n_s	-0.13	—	0.11	-0.02	-0.05	0.16
H_0	0.09	0.11	—	0.80	-0.92	-0.08
ω_b	0.00	-0.02	0.80	—	0.71	0.00
ω_{cdm}	0.10	-0.05	-0.92	0.71	—	-0.11
τ_{reio}	0.98	0.16	-0.08	0.00	-0.11	—

Table 1: Pearson correlations (top) and partial correlations (bottom) between the standard six parameters in ΛCDM with the dataset **CMB-P(EE)+B+SN**. The correlations between τ_{reio} and H_0 are highlighted in bold.

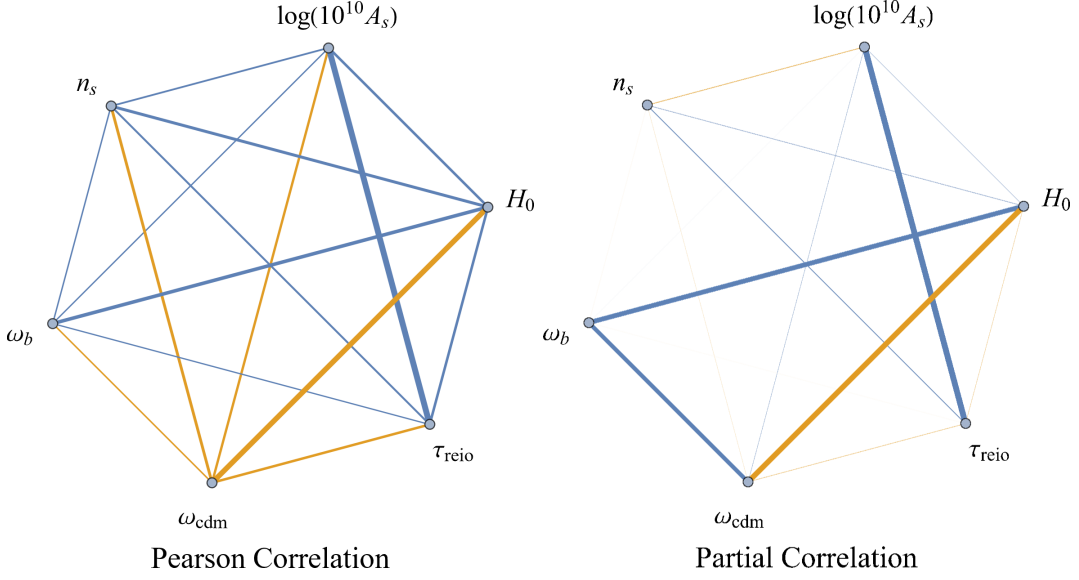


Figure 2: Pearson correlations (left) and partial correlations (right) between parameters in Λ CDM, with the dataset **CMB-P(EE)+B+SN**. Blue lines indicate positive correlations, orange lines indicate negative, and the line thickness is broadcast to a linear scale of the correlation strength.

3.1 Hubble Tension

Let us first discuss the impact of τ_{reio} on the Hubble tension. As has been observed in our previous work [34], τ_{reio} has a mild positive correlation with the Hubble constant H_0 in Λ CDM, as well as in some popular scenarios to relieve the Hubble tension. Here we focus on Λ CDM, with the standard set of six parameters: A_s is the amplitude of primordial scalar fluctuations, n_s the scalar spectral index, H_0 the Hubble expansion rate today, $\Omega_b h^2 \equiv \omega_b$ the baryon density today with $h = H_0/100$, $\Omega_{\text{cdm}} h^2 \equiv \omega_{\text{cdm}}$ the cold dark matter density today, and τ_{reio} the reionization optical depth. For Λ CDM in this work, we treat neutrinos as three degenerate mass eigenstates with total mass $\sum m_\nu = 0.06$ eV (we allow for the neutrino mass sum to be a free parameter in Section 3.3.) Due to the positive $\tau_{\text{reio}}-H_0$ correlation, with the removal of low- ℓ EE data and the resulting larger inferred value of τ_{reio} , H_0 increases mildly and the significance of the Hubble tension is reduced. This can be seen from Figure 1. In the figure, for either **CMB-P** or **CMB-PAS**, without low- ℓ EE data, the positive correlation between τ_{reio} and H_0 is more evident, together with simultaneously enhanced τ_{reio} and H_0 (to a lesser degree).

In order to evaluate the nature of this correlation, we compute the Pearson correlations as well as the (intrinsic) partial correlations between each pair of Λ CDM model parameters when fit to the **CMB-P(EE)+B+SN** dataset⁵, reported in Table 1 (see Section A for correlations when using **CMB-PAS**). First, one can observe that the Pearson correlation between

⁴The relation of Eq. (2.4) is mathematical and independent of the data details. However, it works best when the data is sufficiently Gaussian. In this case, the partial correlation obtained will be close to its original meaning, namely the Pearson correlation of the parameters of interest with all other parameters fixed. This condition is satisfied by the cosmological MC samples, as we will see below in Section 3.

⁵We focus on the correlation coefficients for the **CMB-P(EE)+B+SN** dataset for most of this work. For **CMB-P+B+SN**, the correlations remain qualitatively similar.

τ_{reio} and H_0 is moderate and positive, with a value of 0.43 as shown in bold. However, when computing the partial correlations, we can see that the correlation between H_0 and τ_{reio} more or less vanishes, with a value of -0.08 , indicating that this is not an intrinsic relationship. Rather, the correlation must be carried through a series of correlations between τ_{reio} and other parameters.

One can also visualize these relationships through the correlation diagrams in Figure 2. Here, we depict the Pearson correlations on the left and the partial correlations on the right. Blue lines indicate positive correlations, orange lines indicate negative, and the line thickness is broadcast to a linear scale of the correlation strength. Focusing on the partial correlations on the right-hand side of Figure 2, one can draw paths from τ_{reio} to H_0 passing through other parameters to try to recreate the positive relationship between the two. For instance, the path $\tau_{\text{reio}} \rightarrow n_s \rightarrow H_0$ involves all positive partial correlations, and would contribute to the positive Pearson correlation between τ_{reio} and H_0 . Similarly, a path involving $\tau_{\text{reio}} \rightarrow \omega_{\text{cdm}} \rightarrow H_0$ involves two negative partial correlations and would thus also contribute positively to the overall relationship between H_0 and τ_{reio} . Notably, some paths in the correlation-space will also contribute negatively to the correlation between H_0 and τ_{reio} , e.g. the path $\tau_{\text{reio}} \rightarrow \omega_{\text{cdm}} \rightarrow \omega_b \rightarrow H_0$.⁶ Ultimately, paths with stronger correlations will contribute more significantly, resulting in the overall positive Pearson correlation between τ_{reio} and H_0 .

Using the partial correlation coefficients and the correlation diagrams, then, one can clearly see that the correlation of τ_{reio} and H_0 within the data considered involves many parameters and is not an intrinsic characteristic of these parameters. Nonetheless, a larger inferred value of τ_{reio} still results in a shift in H_0 and a mild reduction of the Hubble tension.

3.2 BAO-CMB Tension

We now wish to comment on the mild tension between CMB datasets and the recent DESI BAO data. BAO is able to directly probe the expansion history of universe by constraining the total matter density today Ω_m , and the product hr_d , with $h = H_0/100$ and r_d the physical size of the sound horizon at the baryon drag epoch. As pointed out in [26, 58], there is a mild discrepancy between inferences from the CMB and from DESI BAO in this parameter space. The authors of [36] pointed out that this anomaly can also be correlated with the optical depth τ_{reio} . In Figure 3, the tension between CMB and BAO data in these parameters could be visualized. One can see that the removal of the low- ℓ EE data and resulting increase in the inferred value of τ_{reio} lessens the tension, as the orange 2σ contour shifts to the black dashed 2σ contour, closer to the gray contours from DESI data alone.

Investigating the nature of the correlations between τ_{reio} and the parameters Ω_m and hr_d , we once more compute the set of Pearson correlations and partial correlations, reported in Table 2 (see Section A for correlations when using **CMB-PAS**). For the purposes of computing partial correlations, the set of parameters which are included is important as it determines which correlations are “factored out” from each intrinsic relationship. For this reason, we choose a set of parameters which includes the parameters of interest $\{\Omega_m, hr_d\}$ and is complementary to the set of free Λ CDM parameters. Thus, the parameter set is $\{\log(10^{10} A_s), n_s, hr_d, \omega_b, \Omega_m, \tau_{\text{reio}}\}$.

⁶Interestingly, the tight Pearson correlation between $\log(10^{10} A_s)$ and τ_{reio} suggests that partial correlations of τ_{reio} with any parameter X should be very small and opposite to the correlation of $\log(10^{10} A_s)$ with X (mostly canceling in Eq. (2.3)), as evident in Table 1.

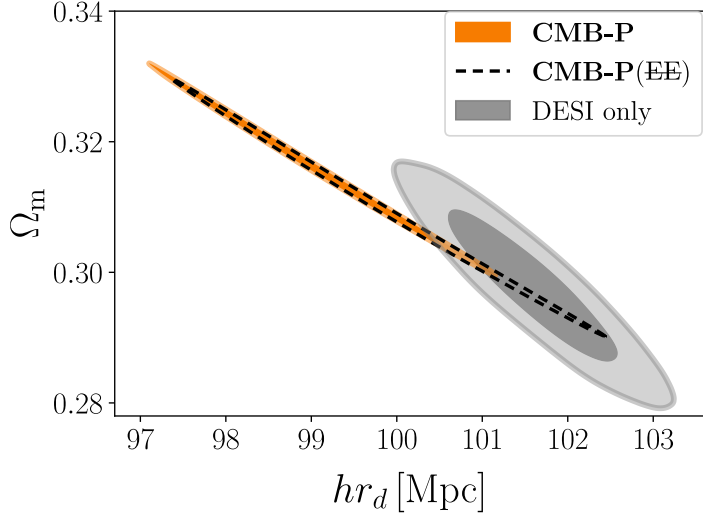


Figure 3: Two-dimensional posterior distribution of Ω_m and hr_d in Λ CDM. The 95% C.L. constraints using the **CMB-P** and **CMB-P(EE)** datasets are depicted in the orange and black dashed contours, respectively, while the 68% (95%) C.L. constraints from DESI only are given by the dark (light) gray contours.

Pearson	$\log(10^{10}A_s)$	n_s	hr_d [Mpc]	ω_b	Ω_m	τ_{reio}
$\log(10^{10}A_s)$	1.00	0.30	0.43	0.23	-0.43	0.98
n_s	0.30	1.00	0.50	0.23	-0.50	0.33
hr_d [Mpc]	0.43	0.50	1.00	0.38	-1.00	0.44
ω_b	0.23	0.23	0.38	1.00	-0.43	0.22
Ω_m	-0.43	-0.50	-1.00	-0.43	1.00	-0.44
τ_{reio}	0.98	0.33	0.44	0.22	-0.44	1.00

Partial	$\log(10^{10}A_s)$	n_s	hr_d [Mpc]	ω_b	Ω_m	τ_{reio}
$\log(10^{10}A_s)$	—	-0.13	0.10	0.15	0.10	0.98
n_s	-0.13	—	0.02	0.03	-0.00	0.16
hr_d [Mpc]	0.10	0.02	—	-0.71	-1.00	-0.10
ω_b	0.15	0.03	-0.71	—	-0.73	-0.15
Ω_m	0.10	-0.00	-1.00	-0.73	—	-0.10
τ_{reio}	0.98	0.16	-0.10	-0.15	-0.10	—

Table 2: Pearson correlations (top) and partial correlations (bottom) between the parameters in the set $\{\log(10^{10}A_s), n_s, hr_d, \omega_b, \Omega_m, \tau_{\text{reio}}\}$ of Λ CDM, with the dataset **CMB-P(EE)+B+SN**. The correlations between τ_{reio} and hr_d (Ω_m) are highlighted in bold.

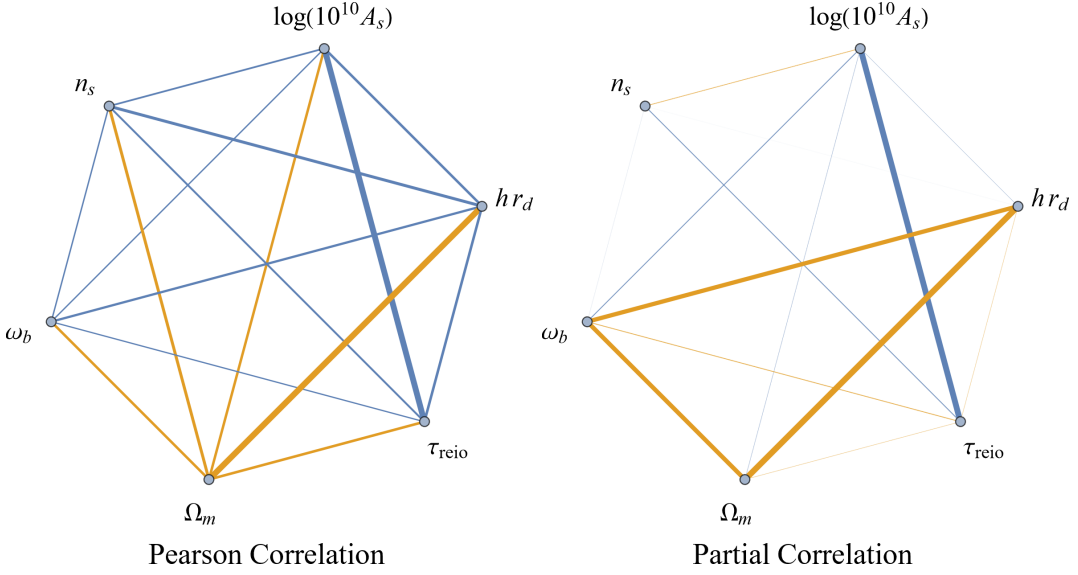


Figure 4: Pearson correlations (left) and partial correlations (right) between any two parameters of the set $\{\log(10^{10}A_s), n_s, h_{rd}, \omega_b, \Omega_m, \tau_{reio}\}$ in Λ CDM, with the dataset **CMB-P(EE)+B+SN**. The plotting style is the same as in Figure 2.

First, one can see clearly the Pearson correlations responsible for the relaxation of this tension. There is a positive correlation between τ_{reio} with h_{rd} of 0.44, and a negative correlation between τ_{reio} and Ω_m of -0.44 . These directions bring the inferences from the full dataset into closer agreement with the inferences made using only the DESI BAO data. Examining, instead, the partial correlations, one sees once more that the relationship between this tension and τ_{reio} is not intrinsic to the parameters themselves, as the partial correlations are quite small. In the case of h_{rd} , the correlation with τ_{reio} is no longer in the correct direction switching from positive to negative. We can visualize these correlations in Figure 4. The Pearson correlations of τ_{reio} and $\{\Omega_m, h_{rd}\}$ can be reconstructed with the partial correlations of other parameters. For example, the positive correlation of h_{rd} and τ_{reio} receives a contribution from the path $\tau_{reio} \rightarrow \omega_b \rightarrow h_{rd}$, which contains two negative correlations and contributes positively.

Thus, similar to the Hubble tension in the previous section, we find a tension in data which is correlated with τ_{reio} and is mildly alleviated by larger values of τ_{reio} . Again this relationship is found to be quite indirect, with the behavior of the other Λ CDM parameters being crucial to explain the overall correlation.

3.3 Neutrino Mass Tension

Another anomalous finding in recent cosmological data, the tight constraints on the sum of neutrino masses $\sum m_\nu$, is also correlated with τ_{reio} . In the context of adding the neutrino mass sum (with a prior $\sum m_\nu > 0$) as one additional parameter to Λ CDM, which we will refer to as Λ CDM+ $\sum m_\nu$, upper bounds on $\sum m_\nu$ involving the newest BAO data from DESI DR2 [26] are in tension with lower bounds from neutrino oscillation experiments, about 0.06 eV for the normal hierarchy case and 0.1 eV for the inverted hierarchy case [27].

As pointed out in [35, 36], an increase in τ_{reio} can alleviate this tension slightly. This could be seen from Figure 5: when the low- ℓ EE data is removed, τ_{reio} increases together

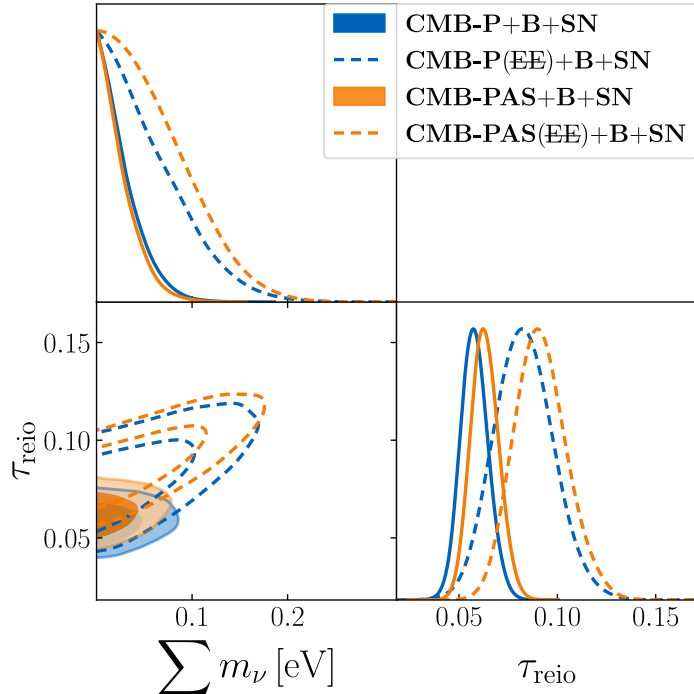


Figure 5: The one- and two-dimensional posterior distributions of τ_{reio} and $\sum m_\nu$ in a series of fits to four different combinations of datasets, assuming the $\Lambda\text{CDM} + \sum m_\nu$ model.

with a relaxation of the upper bound on $\sum m_\nu$. The bound relaxes to $\sum m_\nu < 0.13$ eV for **CMB-P(EE)+B+SN**, easily accommodating lower bounds from neutrino oscillations experiments. Of particular interest is that, with the addition of ACT and SPT CMB observations, the constraint on $\sum m_\nu$ inferred from the **CMB-PAS(EE)+B+SN** dataset relaxes further to $\sum m_\nu < 0.14$ eV, and the posterior starts to form a peak. Although this peak does not constitute a statistically significant lower bound, it suggests that a larger inferred τ_{reio} could indeed lead to detection of a nonzero neutrino mass sum with future updates to CMB observations. In addition, it has been shown in the literature [59, 60] that the constraints on neutrino mass are sensitive to the choice of supernovae dataset. In Section B, we present similar results when using the **SN_{DES}** dataset, showing a posterior with a slightly more prominent peak away from zero neutrino mass sum.

Similar to before, we assess the correlations of τ_{reio} by computing the Pearson and partial correlations of the parameters in the $\Lambda\text{CDM} + \sum m_\nu$ model, shown in Table 3 (see Section A for correlations when using **CMB-PAS**). As expected according to its definition, the partial correlation between the six ΛCDM parameters remain largely intact in Table 1 and Table 3. In other words, the inclusion of Σm_ν in the fit has been properly factored out when obtaining partial correlations. We can also see that while the Pearson correlation between τ_{reio} and $\sum m_\nu$ is relatively strong at 0.58, it becomes small and negative when considering the partial

Pearson	$\log(10^{10} A_s)$	n_s	H_0	ω_b	ω_{cdm}	τ_{reio}	$\sum m_\nu$
$\log(10^{10} A_s)$	1.00	0.47	0.02	0.34	-0.63	0.99	0.60
n_s	0.47	1.00	0.21	0.32	-0.60	0.48	0.41
H_0	0.02	0.21	1.00	0.40	-0.32	0.03	-0.45
ω_b	0.34	0.32	0.40	1.00	-0.36	0.32	0.27
ω_{cdm}	-0.63	-0.60	-0.32	-0.36	1.00	-0.63	-0.63
τ_{reio}	0.99	0.48	0.03	0.32	-0.63	1.00	0.58
$\sum m_\nu$	0.60	0.41	-0.45	0.27	-0.63	0.58	1.00

Partial	$\log(10^{10} A_s)$	n_s	H_0	ω_b	ω_{cdm}	τ_{reio}	$\sum m_\nu$
$\log(10^{10} A_s)$	—	-0.13	0.09	0.01	0.09	0.98	0.15
n_s	-0.13	—	0.08	0.01	-0.07	0.16	0.09
H_0	0.09	0.08	—	0.80	-0.92	-0.09	-0.96
ω_b	0.01	0.01	0.80	—	0.70	-0.00	0.76
ω_{cdm}	0.09	-0.07	-0.92	0.70	—	-0.11	-0.92
τ_{reio}	0.98	0.16	-0.09	-0.00	-0.11	—	-0.13
$\sum m_\nu$	0.15	0.09	-0.96	0.76	-0.92	-0.13	—

Table 3: Pearson correlations (top) and partial correlations (bottom) between parameters of Λ CDM+ $\sum m_\nu$, with the dataset **CMB-P(EE)+B+SN**. The correlations between τ_{reio} and $\sum m_\nu$ (H_0) are highlighted in bold.

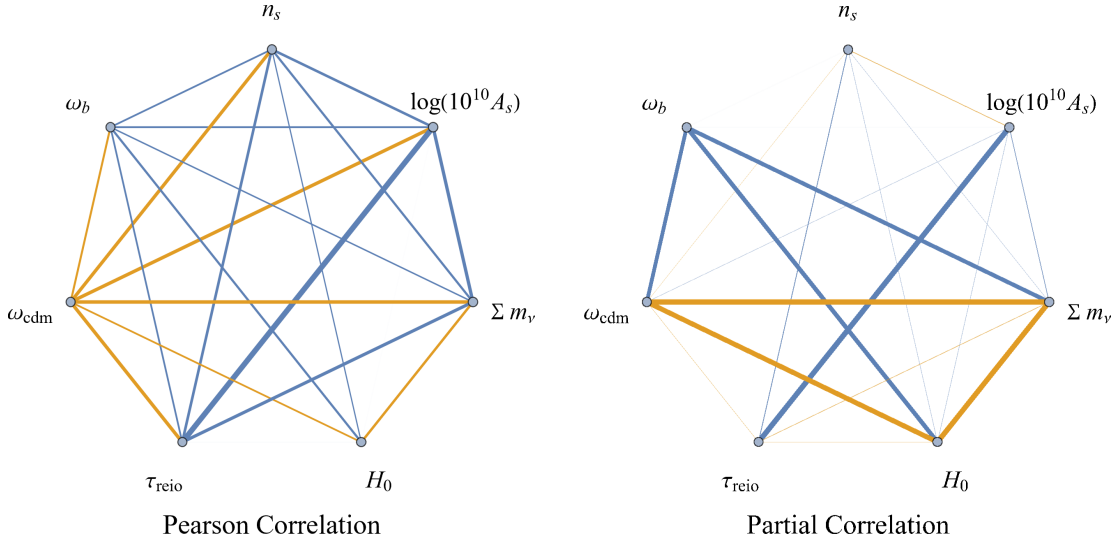


Figure 6: Pearson correlations (left) and partial correlations (right) between parameters of Λ CDM plus $\sum m_\nu$, with the dataset **CMB-P(EE)+B+SN**. The plotting style is the same as in Figure 2.

correlation. Thus, this alleviation of the neutrino-mass tension by a larger τ_{reio} is an indirect effect relating to other parameters of the model. Examining Figure 6, one can attempt to construct the parameter relationships that are responsible for the eventual relationship between τ_{reio} and $\sum m_\nu$. For instance, the path $\tau_{\text{reio}} \rightarrow \omega_{\text{cdm}} \rightarrow \sum m_\nu$ contributes positively.

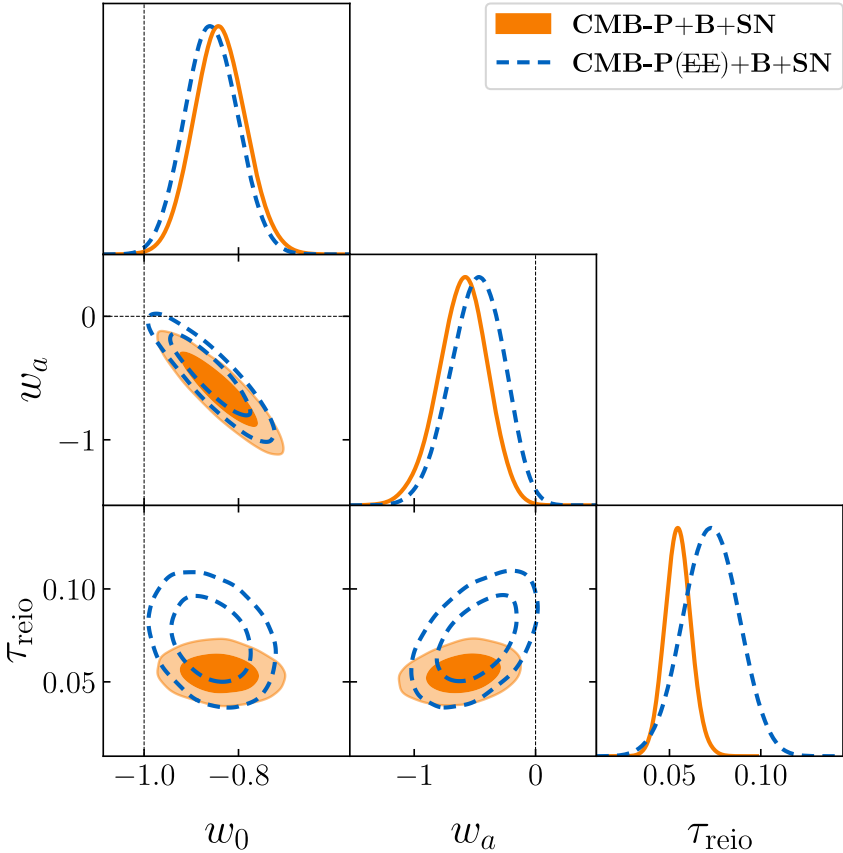


Figure 7: The one- and two-dimensional posterior distributions of τ_{reio} , w_0 , and w_a in a series of fits to two different combinations of datasets, assuming the w_0w_a CDM model.

Yet another interesting observation can be made when examining the correlations of H_0 in this model. Note that H_0 and $\sum m_\nu$ are tightly negatively correlated, both in the Pearson correlation (-0.45) and especially in the partial correlation (-0.96). Meanwhile, as discussed in Section 3.1, H_0 and τ_{reio} are positively correlated in the Λ CDM model. Interestingly, this positive correlation is functionally erased by the strong anti-correlation between H_0 and $\sum m_\nu$, such that in the Λ CDM+ $\sum m_\nu$ model, τ_{reio} does not correlate with H_0 appreciably. This seems to suggest that the ultimate correlations of τ_{reio} with either H_0 or $\sum m_\nu$ rely on similar parameters, while the correlation between τ_{reio} with $\sum m_\nu$ is somewhat stronger such that the $\tau_{\text{reio}}-H_0$ correlation doesn't survive when $\sum m_\nu$ is a free parameter.

3.4 Nature of Dark Energy

In addition to the tensions/anomalies discussed so far, recent analyses involving the BAO measurements from DESI in combination with several datasets of supernovae have challenged the cosmological constant paradigm for DE. Rather than a constant vacuum-energy-like component Λ , there is mild-to-moderate evidence in the data for a dynamical nature of DE. One widely-studied parameterization, the CPL parameterization, assumes the equation of state of dark energy is $w(a) = w_0 + w_a(1 - a)$, where w_0 , w_a are constants, a is the scale factor, and $(w_0, w_a) = (-1, 0)$ corresponds to a cosmological constant DE. Depending on

Pearson	$\log(10^{10} A_s)$	n_s	H_0	ω_b	ω_{cdm}	τ_{reio}	w_0	w_a
$\log(10^{10} A_s)$	1.00	0.52	-0.04	0.45	-0.66	0.99	-0.29	0.49
n_s	0.52	1.00	0.00	0.43	-0.66	0.53	-0.27	0.45
H_0	-0.04	0.00	1.00	0.08	0.05	-0.04	-0.54	0.16
ω_b	0.45	0.43	0.08	1.00	-0.51	0.44	-0.19	0.36
ω_{cdm}	-0.66	-0.66	0.05	-0.51	1.00	-0.66	0.34	-0.62
τ_{reio}	0.99	0.53	-0.04	0.44	-0.66	1.00	-0.28	0.48
w_0	-0.29	-0.27	-0.54	-0.19	0.34	-0.28	1.00	-0.89
w_a	0.49	0.45	0.16	0.36	-0.62	0.48	-0.89	1.00

Partial	$\log(10^{10} A_s)$	n_s	H_0	ω_b	ω_{cdm}	τ_{reio}	w_0	w_a
$\log(10^{10} A_s)$	—	-0.10	0.06	0.04	0.07	0.98	0.07	0.08
n_s	-0.10	—	0.07	0.04	-0.10	0.13	0.06	0.07
H_0	0.06	0.07	—	0.76	-0.89	-0.06	-0.99	-0.98
ω_b	0.04	0.04	0.76	—	0.64	-0.02	0.76	0.76
ω_{cdm}	0.07	-0.10	-0.89	0.64	—	-0.09	-0.91	-0.92
τ_{reio}	0.98	0.13	-0.06	-0.02	-0.09	—	-0.06	-0.07
w_0	0.07	0.06	-0.99	0.76	-0.91	-0.06	—	-1.00
w_a	0.08	0.07	-0.98	0.76	-0.92	-0.07	-1.00	—

Table 4: Pearson correlations (top) and partial correlations (bottom) between parameters in w_0w_a CDM, with the dataset **CMB-P(EE)+B+SN**. The correlations between τ_{reio} and w_0 (w_a) are highlighted in bold.

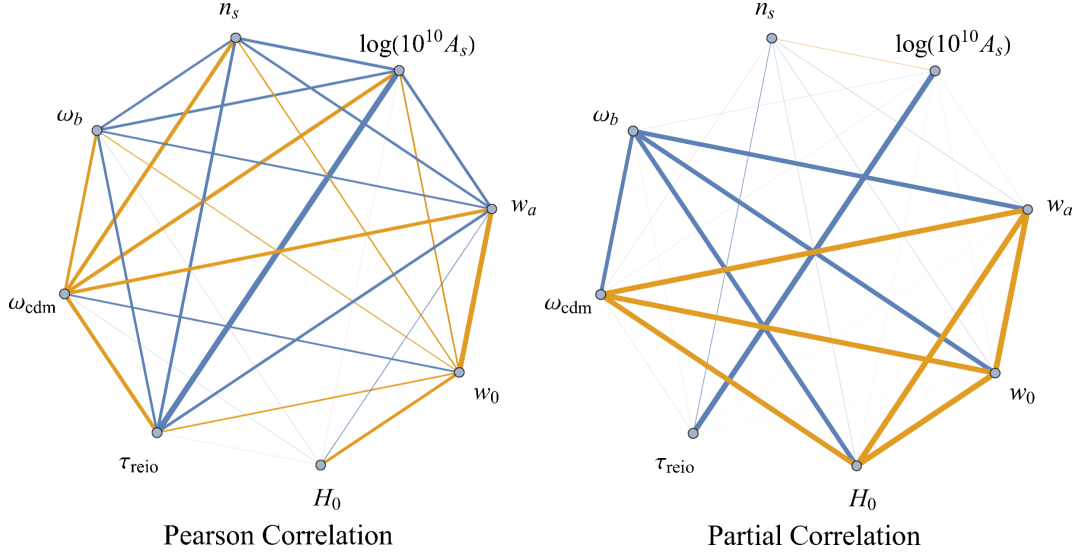


Figure 8: Pearson correlations (left) and partial correlations (right) between parameters of w_0w_a CDM, with the dataset **CMB-P(EE)+B+SN**. The plotting style is the same as in Figure 2.

the choice of supernovae dataset, DESI BAO data leads to an approximately $2\text{-}4\sigma$ evidence for deviations from a cosmological constant, or equivalently (w_0, w_a) departing from $(-1, 0)$

[26, 61].

The authors of [36] pointed out that this behavior may also be mildly correlated with the optical depth τ_{reio} . Focusing on the CPL parameterization, which we will refer to as the $w_0 w_a$ CDM model, we present posteriors in Figure 7 demonstrating that the deviation from Λ CDM is marginally reduced with a larger τ_{reio} (by switching from the **CMB-P+B+SN** to **CMB-P(EE)+B+SN** dataset). We present the correlations in Table 4 and Figure 8. One can remark yet again that the mild-to-moderate Pearson correlations of w_0 and w_a with τ_{reio} are almost absent in the partial correlations, suggesting an indirect nature to this relationship. More specifically, the partial correlation between τ_{reio} and w_0 as well as w_a are both negative and small. Yet through all possible combinations of paths in the partial correlation diagram, the Pearson correlation between τ_{reio} and w_a becomes enhanced and positive while the $\tau_{\text{reio}} - w_0$ correlation remains negative but also enhanced in its absolute value. We find that replacing the supernovae dataset **SN** by either **SN_{DES}** or **SN_{Union3}** does not alter the correlations significantly, even if it changes the significance of detecting dynamical DE (see Section C for more details).

Another interesting feature is the similarity between w_0 and w_a , which is most obvious in the partial correlations. In particular, the partial correlations between w_0/w_a and other cosmological parameters are almost identical to each other. This suggests that in the data, the perturbations of w_0 and w_a around the best fit point are highly indistinguishable, suggesting that the data are most sensitive to a linear combination of w_0 and w_a , rather than each parameter individually. This point can also be seen in the extreme partial correlation of ~ -0.997 between w_0 and w_a . Turning to the physical meaning, we can remark that the equation of state of DE is indeed a linear combination of w_0 and w_a for a given redshift. Thus, the tightness of their correlation suggests that the inferred results are most sensitive to a narrow range of redshifts, corresponding to a particular linear combination. However, this twin-behavior between w_0 and w_a is less obvious in the Pearson correlations, which is also due to the strong negative partial correlation between w_0 and w_a . For any cosmological parameter X , its Pearson correlation with w_0 receives contributions from the partial correlation $w_0 \rightarrow X$ and the path through w_a , *i.e.*, $w_0 \rightarrow w_a \rightarrow X$. The two major contributors will almost cancel each other due to the strong negative partial correlation between w_0 and w_a , such that the Pearson correlation of X with either w_0 or w_a depends instead on small differences and more convoluted paths. Thus, the Pearson correlations end up quite different. The non-trivial relationship between w_0 and w_a can be derived starting from the Pearson correlations, but it is far from apparent from this point of view. Such a hidden structure is, again, revealed in the dual description of partial correlations.

4 Effects of Datasets

From the discussion above, we demonstrate that cosmological parameters are correlated in a nested way. Either the Pearson or partial correlations appear as networks between cosmological parameters. Loop structures in, *e.g.*, Figure 2, prevent us from easily identifying the causes and effects among cosmological parameters. In contrast, it is unambiguous to claim that the inclusion or exclusion of a certain dataset causes the cosmological parameters' distributions to change.

In this section, we want to comment on the effects of certain datasets on inferring the cosmological parameters and their correlations. Based on the discussions developed in Section 3, we analyze the effects of a given dataset by combining the MC samples obtained

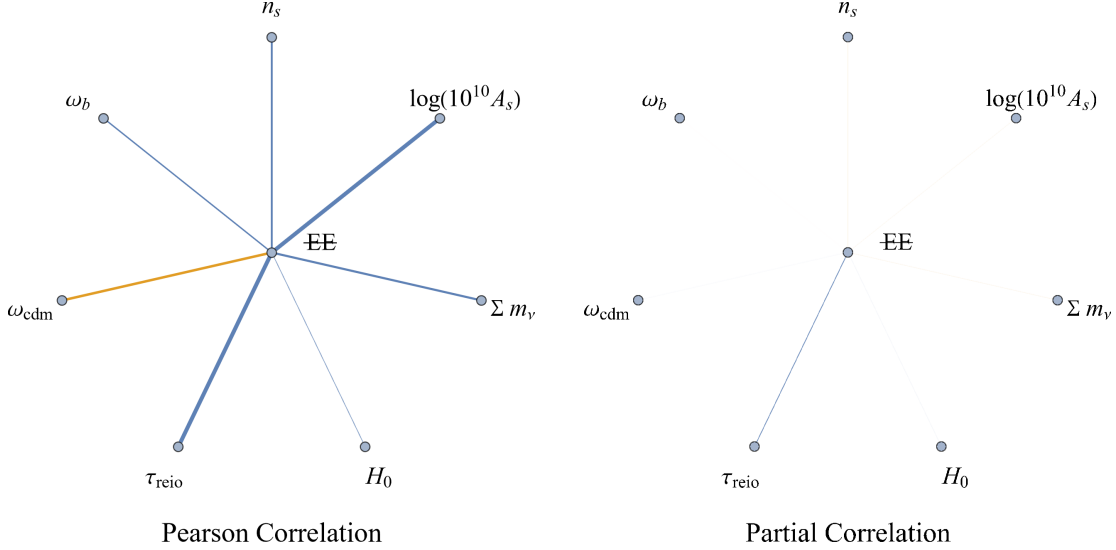


Figure 9: Correlation diagrams highlighting parameter correlations with the exclusion of the low- ℓ EE data of Planck (EE). The left and right panels are the Pearson and partial correlations, respectively. Blue lines indicate positive correlations, orange lines indicate negative, and the line thickness is broadcast to a linear scale of the correlation strength. See the main text for more details.

with and without that dataset, while properly labeling each point in the sample as either including the dataset of interest, or not. By treating the dataset label as a binary parameter of the MC sample, one can calculate the Pearson and partial correlation between this binary parameter and other cosmological parameters.⁷

We first show the impact of excluding the low- ℓ EE data from Planck to all six cosmological parameters of Λ CDM, plus the total neutrino mass. A joint MC sample is constructed by taking an equal weight combination of the **CMB-P+B+SN** and the **CMB-P(EE)+B+SN** MC samples. All (EE) samples are labeled with a binary parameter with value one, while the others are labeled with value zero. The Pearson and partial correlations of this binary parameter and other cosmological parameters are calculated, and the results are presented in Figure 9. In both panels, only the correlation between the binary (EE) parameter and other cosmological parameters is shown, with the former node placed in the middle of each panel for better display. The Pearson correlation directly describes the effect of excluding the low- ℓ EE data. For instance, if using the **CMB-P(EE)** dataset increases a parameter such as τ_{reio} , the Pearson correlation between τ_{reio} and the binary label parameter is then positive; if the result is to decrease the parameter, the correlation is negative. The left panel of Figure 9 shows that excluding the low- ℓ EE data affects all cosmological parameters, with most of them trending towards larger values, except for ω_{cdm} . The point has been thoroughly discussed in [34] and [17]. On the contrary, in the dual view of partial correlations, the effect of (EE) dataset is more straightforward to be understood. As first pointed out by [34] and also in Section 3, excluding the low- ℓ EE data does not affect most cosmological parameters other than τ_{reio} directly. Instead, the effects are seen as the

⁷The method is inspired by the field of causal inference [62], where the inclusion (exclusion) of a new dataset could be considered as a “treatment” on the cosmology, and the effect of such a treatment can be inferred from the distribution differences of cosmological parameters.

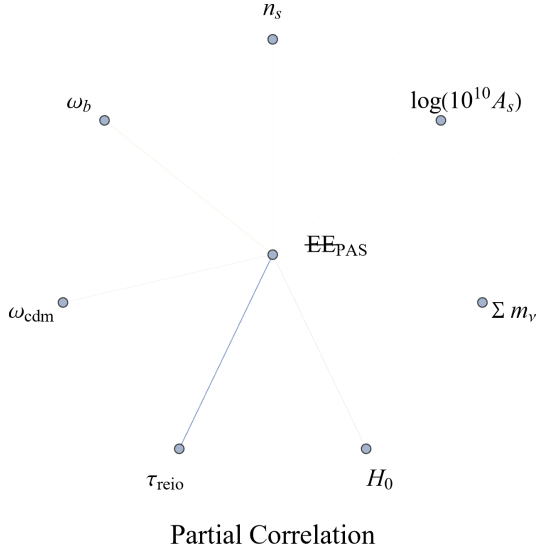


Figure 10: Partial correlation diagram highlighting parameter correlations with the exclusion of the low- ℓ EE data of Planck (EE), within the combination **CMB-PAS+B+SN**. An appreciable correlation is only observed for τ_{reio} , as is the case with **CMB-P**, **CMB-PA**, and **CMB-PS**. The plotting style is the same as Figure 9.

Pearson correlations between the (EE) and cosmological parameters, including A_s , largely stem from increasing τ_{reio} , as demonstrated by the partial correlations in the right panel of Figure 9. Other than τ_{reio} with a partial correlation of 0.16, the binary label parameter of (EE) develops no significant partial correlation with other cosmological parameters, with the second most significant one being with n_s at less than 0.04. The relation strengthens the argument that the low- ℓ EE part of the Planck dataset breaks the degeneracy between A_s and τ_{reio} , constraining the latter to a lower value and then affecting other cosmological parameters. To further validate the points above, we also show the effect of excluding low- ℓ EE data when using the **CMB-PAS** datasets in the same way. The partial correlations are shown in Figure 10. In this case, the direct effect of removing the low- ℓ EE data is highly consistent with the **CMB-P** case, with the leading effect of raising τ_{reio} . We have checked that the same consistency is seen when using **CMB-PA** or **CMB-PS** as well.

Aside from the above, we also checked the correlation between the inclusion of the ACT and SPT datasets with cosmological parameters. In this case, the joint dataset is made of equal weights of **CMB-P(EE)+SN+B** MC samples and either **CMB-PA(EE)+SN+B** or **CMB-PS(EE)+SN+B** MC samples. Each MC sample receives a binary ACT (SPT) label with value one if it comes from the **CMB-PA(CMB-PS)** dataset, and zero if not. The Pearson and partial correlations are shown in Figures 11 and 12. Unlike the case of the Planck low- ℓ EE data, these new datasets with a significant amount of information in the high- ℓ modes affect almost all cosmological parameters. Most elements are non-negligible in the views of both Pearson and partial correlations. Moreover, the effects of the ACT and SPT data are similar to each other in both Pearson and partial correlations, strongly indicating the consistency of the high- ℓ data impact. Both datasets tend to increase the value of n_s . The increase of n_s remains obvious in terms of partial correlation, where the effects from other cosmological parameters are excluded. Similar positive correlations also appear in A_s and ω_b . Situations for the remaining four parameters are less straightforward, as the impact

in terms of Pearson and partial correlations are often of the opposite sign.

Finally, we also investigate briefly the affects of different supernovae datasets, **SN**, **SN_{DES}**, and **SN_{Union3}**, in particular in the dynamical DE context. The cosmological parameter correlations remain qualitatively similar to the **SN** MC samples presented in Section 3.4 (see Section C for the correlation coefficients for **SN_{DES}** and **SN_{Union3}**.)

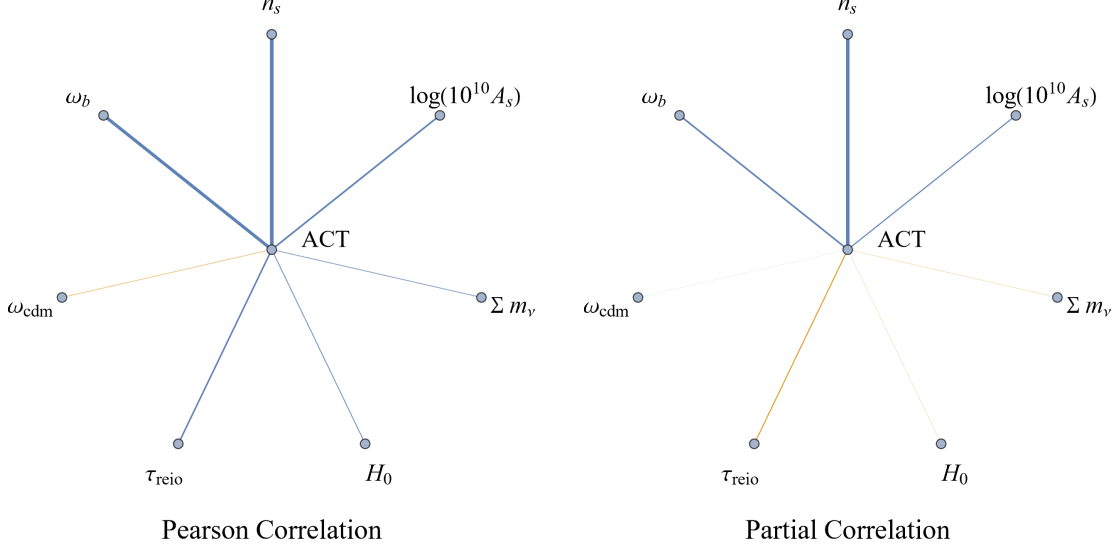


Figure 11: Correlation diagrams highlighting parameter correlations with the inclusion of ACT data. The left and right panels are the Pearson and partial correlations, respectively. The plotting style is the same as Figure 9.

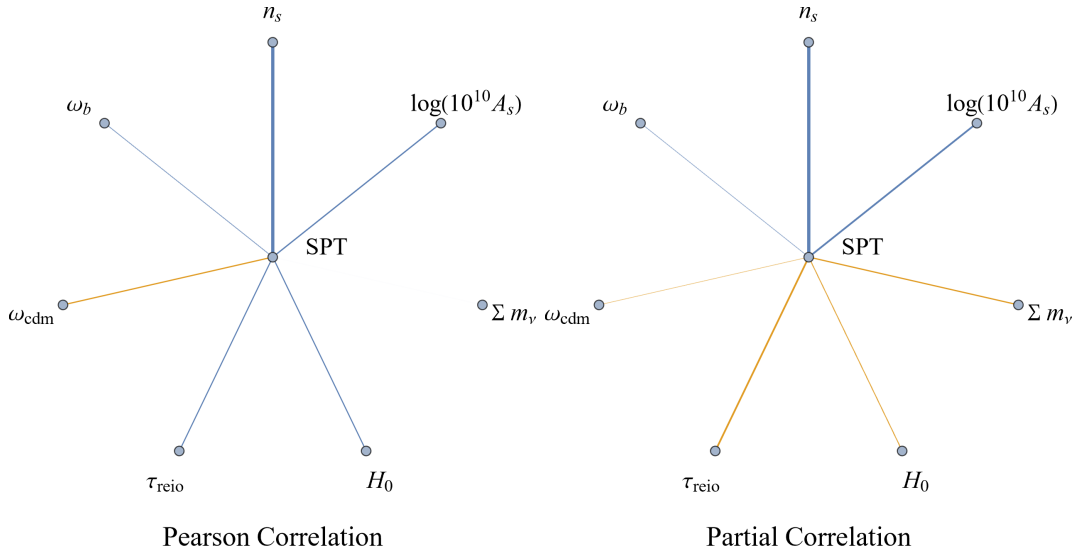


Figure 12: Correlation diagrams highlighting parameter correlations with the inclusion of SPT data. The left and right panels are the Pearson and partial correlations, respectively. The plotting style is the same as Figure 9.

5 Conclusion

A nontrivial relationship between constraints on the optical depth of reionization τ_{reio} from CMB data and various tensions and anomalies in cosmology has begun to be uncovered. In our own recent work [34] and that of others [35, 36], a potential increase in the inferred value of τ_{reio} has been shown to alleviate tensions between several sets of data in cosmology. In this work, we have explored discrepancies between (i) CMB and supernovae determinations of H_0 , (ii) CMB and BAO constraints on Ω_m and h_{rd} , (iii) cosmological upper bounds and experimental lower bounds on $\sum m_\nu$, and (iv) inferences of dynamical dark energy or a cosmological constant. We have summarized the behavior that follows from larger τ_{reio} in each context and taken a further step to investigate the parameter relationships responsible for these shifts in tension.

By analyzing the correlations of different sets of cosmological parameters within each model and dataset of interest, we have been able to further uncover the nature of these relationships. The Pearson correlation coefficients in Tables 1 to 4 clearly display that, for each tension/anomaly, τ_{reio} is correlated with the appropriate parameters such that an increase in τ_{reio} would relax the tension. In contrast, the partial correlation coefficients in the same tables demonstrate that each correlation with τ_{reio} is not intrinsic to that parameter, as the values of the partial correlations of interest tend to be close to zero. Rather, our analysis has shown that the significant Pearson correlations with τ_{reio} are a consequence of several many-dimensional parameter relationships. We can therefore conclude that, while a potential increase in τ_{reio} could relax and even relieve some of the tensions we discussed, this behavior is not a property of τ_{reio} itself.

It is interesting also to consider the likelihood of such a shift in the observed value of τ_{reio} . In this work, we have periodically excluded the low- ℓ EE dataset from the *Planck* CMB data as a proxy for inferring larger τ_{reio} . However, an important question remains of whether such a shift in τ_{reio} is likely to happen. At this point, only the low- ℓ data from *Planck* serves to break the parameter degeneracy between the primordial spectrum amplitude A_s and τ_{reio} , and thus this one set of data from a single experiment provides the most up-to-date CMB constraints on τ_{reio} . There is some effort to provide complementary observations, with some progress already made by ground-based experiments such as CLASS [63], AliCPT [64] and future observations to be made by satellite telescopes such as *LiteBIRD* [65]. These will serve as independent checks on the CMB spectra at the largest scales, providing more input to the constraints on τ_{reio} . As of now, there are no significant reasons to doubt the constraints from *Planck* (see e.g. [66] for a recent analysis using the latest data from *Planck* PR4). However, the low- ℓ EE part of the *Planck* spectra has the largest statistical uncertainties. Future data will improve on the precision and provide more robust constraints on τ_{reio} . Thus, it may be interesting to see in the coming years whether a shift in τ_{reio} is observed, and how it would impact the biggest puzzles in cosmology.

Acknowledgements

We would like to thank Elisa Ferreira and Joel Meyers for helpful discussions. IJA, JF and PS are supported by the NASA grant 80NSSC22K081 and the DOE grant DE-SC-0010010. This work was conducted using computational resources and services at the Center for Computation and Visualization, Brown University.

References

- [1] S. Dodelson, *Modern Cosmology*, Academic Press, Amsterdam (2003).
- [2] B.E. Robertson, R.S. Ellis, S.R. Furlanetto and J.S. Dunlop, *Cosmic Reionization and Early Star-forming Galaxies: a Joint Analysis of new Constraints From Planck and the Hubble Space Telescope*, *Astrophys. J. Lett.* **802** (2015) L19 [[1502.02024](#)].
- [3] M. McQuinn, *The Evolution of the Intergalactic Medium*, *Ann. Rev. Astron. Astrophys.* **54** (2016) 313 [[1512.00086](#)].
- [4] PLANCK collaboration, *Planck 2018 results. VI. Cosmological parameters*, *Astron. Astrophys.* **641** (2020) A6 [[1807.06209](#)].
- [5] P. Jakobsen, P. Ferruit, C. Alves de Oliveira, S. Arribas, G. Bagnasco, R. Barho et al., *The near-infrared spectrograph (nirspec) on the James Webb space telescope: I. overview of the instrument and its capabilities*, *Astronomy & Astrophysics* **661** (2022) A80.
- [6] G.S. Wright, G.H. Rieke, A. Glasse, M. Ressler, M. García Marín, J. Aguilar et al., *The Mid-infrared Instrument for JWST and Its In-flight Performance*, *Publications of the ASP* **135** (2023) 048003.
- [7] J.B. Muñoz, J. Mirocha, J. Chisholm, S.R. Furlanetto and C. Mason, *Reionization after JWST: a photon budget crisis?*, *Mon. Not. Roy. Astron. Soc.* **535** (2024) L37 [[2404.07250](#)].
- [8] C. Simmonds, S. Tacchella, K. Hainline, B.D. Johnson, W. McClymont, B. Robertson et al., *Low-mass bursty galaxies in JADES efficiently produce ionising photons and could represent the main drivers of reionisation*, [2310.01112](#).
- [9] R. Endsley, D.P. Stark, L. Whitler, M.W. Topping, B.D. Johnson, B. Robertson et al., *The star-forming and ionizing properties of dwarf $z \sim 6-9$ galaxies in JADES: insights on bursty star formation and ionized bubble growth*, *Monthly Notices of the RAS* **533** (2024) 1111 [[2306.05295](#)].
- [10] S.L. Finkelstein, G.C.K. Leung, M.B. Bagley, M. Dickinson, H.C. Ferguson, C. Papovich et al., *The Complete CEERS Early Universe Galaxy Sample: A Surprisingly Slow Evolution of the Space Density of Bright Galaxies at $z \sim 8.5-14.5$* , *Astrophysical Journal, Letters* **969** (2024) L2 [[2311.04279](#)].
- [11] S.L. Finkelstein, M.B. Bagley, H.C. Ferguson, S.M. Wilkins, J.S. Kartaltepe, C. Papovich et al., *Ceers key paper. i. an early look into the first 500 myr of galaxy formation with jwst*, *The Astrophysical Journal Letters* **946** (2023) L13.
- [12] J. Chisholm, A. Saldana-Lopez, S. Flury, D. Schaefer, A. Jaskot, R. Amorín et al., *The far-ultraviolet continuum slope as a Lyman continuum escape estimator at high redshift*, *Monthly Notices of the Royal Astronomical Society* **517** (2022) 5104–5120.
- [13] P. Mukherjee, A. Dey and S. Pal, *What can we learn about Reionization astrophysical parameters using Gaussian Process Regression?*, [2407.19481](#).
- [14] D. Paoletti, D.K. Hazra, F. Finelli and G.F. Smoot, *Evidence for asymmetric reionization histories from a joint analysis of the cosmic microwave background and astrophysical data*, *Phys. Rev. D* **111** (2025) 043532 [[2405.09506](#)].
- [15] Y. Zhu et al., *SMILES: Potentially Higher Ionizing Photon Production Efficiency in Overdense Regions*, *Astrophys. J.* **986** (2025) 18 [[2410.14804](#)].
- [16] C. Cain, G. Lopez, A. D’Aloisio, J.B. Munoz, R.A. Jansen, R.A. Windhorst et al., *Chasing the Beginning of Reionization in the JWST Era*, *Astrophys. J.* **980** (2025) 83 [[2409.02989](#)].
- [17] W. Giarè, E. Di Valentino and A. Melchiorri, *Measuring the reionization optical depth without large-scale CMB polarization*, *Phys. Rev. D* **109** (2024) 103519 [[2312.06482](#)].

- [18] D. Scolnic, A.G. Riess, J. Wu, S. Li, G.S. Anand, R. Beaton et al., *CATS: The Hubble Constant from Standardized TRGB and Type Ia Supernova Measurements*, *Astrophys. J. Lett.* **954** (2023) L31 [[2304.06693](#)].
- [19] A.G. Riess and et al., *A Comprehensive Measurement of the Local Value of the Hubble Constant with $1 \text{ km s}^{-1} \text{ Mpc}^{-1}$ Uncertainty from the Hubble Space Telescope and the SH0ES Team*, *Astrophys. J. Lett.* **934** (2022) L7 [[2112.04510](#)].
- [20] L. Breuval, A.G. Riess, S. Casertano, W. Yuan, L.M. Macri, M. Romanieló et al., *Small Magellanic Cloud Cepheids Observed with the Hubble Space Telescope Provide a New Anchor for the SH0ES Distance Ladder*, *Astrophys. J.* **973** (2024) 30 [[2404.08038](#)].
- [21] W.L. Freedman, *Measurements of the Hubble Constant: Tensions in Perspective*, *Astrophys. J.* **919** (2021) 16 [[2106.15656](#)].
- [22] W.L. Freedman and B.F. Madore, *Progress in direct measurements of the Hubble constant*, *JCAP* **11** (2023) 050 [[2309.05618](#)].
- [23] W.L. Freedman, B.F. Madore, I.S. Jang, T.J. Hoyt, A.J. Lee and K.A. Owens, *Status Report on the Chicago-Carnegie Hubble Program (CCHP): Three Independent Astrophysical Determinations of the Hubble Constant Using the James Webb Space Telescope*, [2408.06153](#).
- [24] H0LiCOW Collaboration, *H0LiCOW - XIII. A 2.4 per cent measurement of H_0 from lensed quasars: 5.3 σ tension between early- and late-Universe probes*, *Mon. Not. Roy. Astron. Soc.* **498** (2020) 1420 [[1907.04869](#)].
- [25] A.G. Riess and et al., *JWST Validates HST Distance Measurements: Selection of Supernova Subsample Explains Differences in JWST Estimates of Local H_0* , *Astrophys. J.* **977** (2024) 120 [[2408.11770](#)].
- [26] DESI collaboration, *DESI DR2 Results II: Measurements of Baryon Acoustic Oscillations and Cosmological Constraints*, [2503.14738](#).
- [27] PARTICLE DATA GROUP collaboration, *Review of particle physics*, *Phys. Rev. D* **110** (2024) 030001.
- [28] DESI collaboration, *Constraints on Neutrino Physics from DESI DR2 BAO and DR1 Full Shape*, [2503.14744](#).
- [29] N. Craig, D. Green, J. Meyers and S. Rajendran, *No νs is Good News*, *JHEP* **09** (2024) 097 [[2405.00836](#)].
- [30] D. Green and J. Meyers, *Cosmological preference for a negative neutrino mass*, *Phys. Rev. D* **111** (2025) 083507 [[2407.07878](#)].
- [31] P.W. Graham, D. Green and J. Meyers, *Dark Forces Gathering*, [2508.20999](#).
- [32] M. Chevallier and D. Polarski, *Accelerating universes with scaling dark matter*, *Int. J. Mod. Phys. D* **10** (2001) 213 [[gr-qc/0009008](#)].
- [33] E.V. Linder, *Exploring the expansion history of the universe*, *Phys. Rev. Lett.* **90** (2003) 091301 [[astro-ph/0208512](#)].
- [34] I.J. Allali, P. Singh, J. Fan and L. Li, *Reionization and the Hubble Constant: Correlations in the Cosmic Microwave Background*, [2503.05691](#).
- [35] T. Jhaveri, T. Karwal and W. Hu, *Turning a negative neutrino mass into a positive optical depth*, [2504.21813](#).
- [36] N. Sailer, G.S. Farren, S. Ferraro and M. White, *Disputable: the high cost of a low optical depth*, [2504.16932](#).
- [37] H. Cheng, Z. Yin, E. Di Valentino, D.J.E. Marsh and L. Visinelli, *Constraining exotic high- z reionization histories with Gaussian processes and the cosmic microwave background*, [2506.19096](#).

- [38] C. Cain, A. Van Engelen, K.S. Croker, D. Kramer, A. D’Aloisio and G. Lopez, *The CMB optical depth constrains the duration of reionization*, [2505.15899](#).
- [39] T. Namikawa, *Resolving the negative neutrino mass with cosmic birefringence*, [2506.22999](#).
- [40] J.C. Tan, *Flash Ionization of the Early Universe by Population III.1 Supermassive Stars*, *Astrophys. J. Lett.* **989** (2025) L47 [[2506.18490](#)].
- [41] PLANCK collaboration, *Planck 2018 results. V. CMB power spectra and likelihoods*, *Astron. Astrophys.* **641** (2020) A5 [[1907.12875](#)].
- [42] G. Efstathiou and S. Gratton, *A detailed description of the camspec likelihood pipeline and a reanalysis of the planck high frequency maps*, *The Open Journal of Astrophysics* **4** (2021) .
- [43] E. Rosenberg, S. Gratton and G. Efstathiou, *Cmb power spectra and cosmological parameters from planck pr4 with camspec*, *Mon. Not. Roy. Astron. Soc.* **517** (2022) 4620–4636.
- [44] PLANCK collaboration, *Planck intermediate results. LVII. Joint Planck LFI and HFI data processing*, *Astron. Astrophys.* **643** (2020) A42 [[2007.04997](#)].
- [45] J. Carron, M. Mirmelstein and A. Lewis, *CMB lensing from Planck PR4 maps*, *JCAP* **09** (2022) 039 [[2206.07773](#)].
- [46] ACT collaboration, *The Atacama Cosmology Telescope: A Measurement of the DR6 CMB Lensing Power Spectrum and Its Implications for Structure Growth*, *Astrophys. J.* **962** (2024) 112 [[2304.05202](#)].
- [47] ACT collaboration, *The Atacama Cosmology Telescope: DR6 Gravitational Lensing Map and Cosmological Parameters*, *Astrophys. J.* **962** (2024) 113 [[2304.05203](#)].
- [48] ACT collaboration, *The Atacama Cosmology Telescope: DR6 Power Spectra, Likelihoods and LambdaCDM Parameters*, [2503.14452](#).
- [49] SPT-3G collaboration, *SPT-3G D1: CMB temperature and polarization power spectra and cosmology from 2019 and 2020 observations of the SPT-3G Main field*, [2506.20707](#).
- [50] D. Scolnic et al., *The Pantheon+ Analysis: The Full Data Set and Light-curve Release*, *Astrophys. J.* **938** (2022) 113 [[2112.03863](#)].
- [51] DES collaboration, *The Dark Energy Survey: Cosmology Results with ~ 1500 New High-redshift Type Ia Supernovae Using the Full 5 yr Data Set*, *Astrophys. J. Lett.* **973** (2024) L14 [[2401.02929](#)].
- [52] D. Rubin et al., *Union Through UNITY: Cosmology with 2,000 SNe Using a Unified Bayesian Framework*, [2311.12098](#).
- [53] J. Lesgourgues, *The Cosmic Linear Anisotropy Solving System (CLASS) I: Overview*, [1104.2932](#).
- [54] D. Blas, J. Lesgourgues and T. Tram, *The Cosmic Linear Anisotropy Solving System (CLASS) II: Approximation schemes*, *JCAP* **07** (2011) 034 [[1104.2933](#)].
- [55] J. Torrado and A. Lewis, *Cobaya: Code for Bayesian Analysis of hierarchical physical models*, *JCAP* **05** (2021) 057 [[2005.05290](#)].
- [56] J. Torrado and A. Lewis, “Cobaya: Bayesian analysis in cosmology.” Astrophysics Source Code Library, record ascl:1910.019, Oct., 2019.
- [57] A. Lewis, *GetDist: a Python package for analysing Monte Carlo samples*, [1910.13970](#).
- [58] E.G.M. Ferreira, E. McDonough, L. Balkenhol, R. Kallosh, L. Knox and A. Linde, *The BAO-CMB Tension and Implications for Inflation*, [2507.12459](#).
- [59] I.J. Allali and A. Notari, *Neutrino mass bounds from DESI 2024 are relaxed by Planck PR4 and cosmological supernovae*, *JCAP* **12** (2024) 020 [[2406.14554](#)].

- [60] M. Loverde and Z.J. Weiner, *Massive neutrinos and cosmic composition*, *JCAP* **12** (2024) 048 [[2410.00090](#)].
- [61] DESI collaboration, *Dynamical Dark Energy in light of the DESI DR2 Baryonic Acoustic Oscillations Measurements*, [2504.06118](#).
- [62] J. Pearl, M. Glymour and N.P. Jewell, *Causal inference in statistics: A primer*, 2016, <https://api.semanticscholar.org/CorpusID:148322624>.
- [63] CLASS collaboration, *A Measurement of the Largest-scale CMB E-mode Polarization with CLASS*, *Astrophys. J.* **986** (2025) 111 [[2501.11904](#)].
- [64] H. Li et al., *Probing Primordial Gravitational Waves: Ali CMB Polarization Telescope*, *Natl. Sci. Rev.* **6** (2019) 145 [[1710.03047](#)].
- [65] LITEBIRD collaboration, *The LiteBIRD mission*, *PoS ICHEP2022* (2022) 085.
- [66] S. Ilic et al., *Reconstructing the epoch of reionisation with Planck PR4*, *Astron. Astrophys.* **700** (2025) A26 [[2504.13254](#)].

Pearson	$\log(10^{10}A_s)$	n_s	H_0	ω_b	ω_{cdm}	τ_{reio}
$\log(10^{10}A_s)$	1.00	0.30	0.45	0.20	-0.44	0.97
n_s	0.30	1.00	0.44	-0.02	-0.49	0.35
H_0	0.45	0.44	1.00	0.49	-0.91	0.46
ω_b	0.20	-0.02	0.49	1.00	-0.19	0.19
ω_{cdm}	-0.44	-0.49	-0.91	-0.19	1.00	-0.45
τ_{reio}	0.97	0.35	0.46	0.19	-0.45	1.00

Partial	$\log(10^{10}A_s)$	n_s	H_0	ω_b	ω_{cdm}	τ_{reio}
$\log(10^{10}A_s)$	—	-0.26	0.09	-0.04	0.05	0.97
n_s	-0.26	—	0.16	-0.21	0.00	0.29
H_0	0.09	0.16	—	0.78	-0.94	-0.08
ω_b	-0.04	-0.21	0.78	—	0.70	0.06
ω_{cdm}	0.05	0.00	-0.94	0.70	—	-0.07
τ_{reio}	0.97	0.29	-0.08	0.06	-0.07	—

Table 5: Pearson correlations (top) and partial correlations (bottom) between the standard six parameters in Λ CDM with the dataset **CMB-PAS(EE)+B+SN**.

A Correlations for CMB-PAS(EE)

We present tables of Pearson and partial correlation coefficients complementary to Tables 1 to 3, using instead the **CMB-PAS(EE)+B+SN** data combination. Table 5 gives correlations for the six Λ CDM parameters; Table 6 shows the parameter set $\{\log(10^{10}A_s), n_s, hrd, \omega_b, \Omega_m, \tau_{\text{reio}}\}$ relevant for the BAO-CMB tension discussion in Section 3.2; and Table 7 gives the correlations for the seven parameters of Λ CDM+ $\sum m_\nu$. The correlations are qualitatively similar to those given in Tables 1 to 3, with the greater fluctuations in the partial correlations compared to the Pearson correlations. In addition, correlations of n_s are slightly altered due to the greater sensitivity to the small-scale power spectrum in ACT/SPT data, especially the correlation between n_s and ω_b which nearly switches direction when replacing **CMB-P** with **CMB-PAS**.

Pearson	$\log(10^{10}A_s)$	n_s	hr_d [Mpc]	ω_b	Ω_m	τ_{reio}
$\log(10^{10}A_s)$	1.00	0.30	0.45	0.20	-0.46	0.97
n_s	0.30	1.00	0.49	-0.02	-0.48	0.35
hr_d [Mpc]	0.45	0.49	1.00	0.30	-1.00	0.46
ω_b	0.20	-0.02	0.30	1.00	-0.34	0.19
Ω_m	-0.46	-0.48	-1.00	-0.34	1.00	-0.46
τ_{reio}	0.97	0.35	0.46	0.19	-0.46	1.00

Partial	$\log(10^{10}A_s)$	n_s	hr_d [Mpc]	ω_b	Ω_m	τ_{reio}
$\log(10^{10}A_s)$	—	-0.26	0.06	0.06	0.06	0.97
n_s	-0.26	—	0.07	-0.12	0.04	0.29
hr_d [Mpc]	0.06	0.07	—	-0.67	-1.00	-0.07
ω_b	0.06	-0.12	-0.67	—	-0.68	-0.05
Ω_m	0.06	0.04	-1.00	-0.68	—	-0.06
τ_{reio}	0.97	0.29	-0.07	-0.05	-0.06	—

Table 6: Pearson correlations (top) and partial correlations (bottom) between the parameters in the set $\{\log(10^{10}A_s), n_s, hr_d, \omega_b, \Omega_m, \tau_{\text{reio}}\}$ in ΛCDM with the dataset **CMB-PAS(EE)+B+SN**.

Pearson	$\log(10^{10}A_s)$	n_s	H_0	ω_b	ω_{cdm}	τ_{reio}	$\sum m_\nu$
$\log(10^{10}A_s)$	1.00	0.50	-0.11	0.27	-0.69	0.98	0.68
n_s	0.50	1.00	0.10	0.06	-0.64	0.53	0.44
H_0	-0.11	0.10	1.00	0.28	-0.21	-0.08	-0.55
ω_b	0.27	0.06	0.28	1.00	-0.27	0.25	0.20
ω_{cdm}	-0.69	-0.64	-0.21	-0.27	1.00	-0.69	-0.65
τ_{reio}	0.98	0.53	-0.08	0.25	-0.69	1.00	0.65
$\sum m_\nu$	0.68	0.44	-0.55	0.20	-0.65	0.65	1.00

Partial	$\log(10^{10}A_s)$	n_s	H_0	ω_b	ω_{cdm}	τ_{reio}	$\sum m_\nu$
$\log(10^{10}A_s)$	—	-0.25	0.11	-0.06	0.07	0.97	0.17
n_s	-0.25	—	0.13	-0.19	-0.04	0.28	0.14
H_0	0.11	0.13	—	0.79	-0.93	-0.10	-0.97
ω_b	-0.06	-0.19	0.79	—	0.69	0.07	0.76
ω_{cdm}	0.07	-0.04	-0.93	0.69	—	-0.09	-0.93
τ_{reio}	0.97	0.28	-0.10	0.07	-0.09	—	-0.15
$\sum m_\nu$	0.17	0.14	-0.97	0.76	-0.93	-0.15	—

Table 7: Pearson correlations (top) and partial correlations (bottom) between the seven parameters in $\Lambda\text{CDM} + \sum m_\nu$ with the dataset **CMB-PAS(EE)+B+SN**.

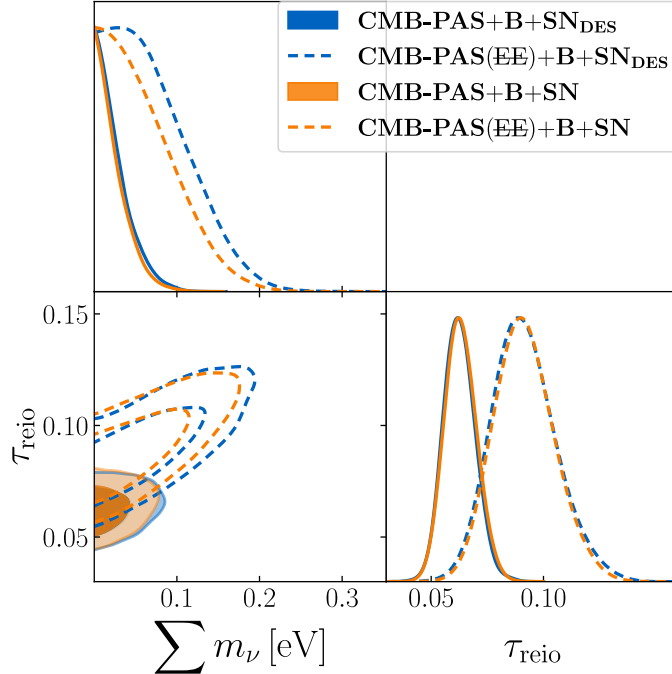


Figure 13: The one- and two-dimensional posterior distributions of τ_{reio} and $\sum m_\nu$ in a series of fits to four different combinations of datasets, assuming the $\Lambda\text{CDM} + \sum m_\nu$ model.

B Neutrino Mass with SN_{DES}

As pointed out in Section 3.3, the combination of *Planck*, ACT, and SPT CMB data, in the absence of the low- ℓ EE data, begins to show a peaked posterior for $\sum m_\nu$. In the case of the data combination **CMB-PAS(EE)+B+SN**, this peak is very marginally present. However, as shown in [59, 60], constraints on neutrino masses depend significantly on the choice of supernovae data. As an example, we present in Figure 13 also a fit using the DES supernovae dataset. One can see that the neutrino mass constraint is most significantly relaxed with the **CMB-PAS(EE)+B+SN_{DES}** dataset, corresponding to $\sum m_\nu < 0.16$ eV at 95% C.L., and indeed this posterior even shows the clear formation of a peak away from zero. In such a context, then, the observation of “negative neutrino mass” is no longer present.

C Correlations for SN_{DES} and $\text{SN}_{\text{Union3}}$ in $w_0 w_a$ CDM

We provide tables of the Pearson and partial correlation coefficients for the $w_0 w_a$ CDM model parameters when fitting to **CMB-P(EE)+B+SN_{DES}** in Table 8 and **CMB-P(EE)+B+SN_{Union3}** in Table 9, analogous to Table 4 displaying the case of **CMB-P(EE)+B+SN**. The correlations are nearly identical, with minor fluctuations, for any given choice of supernovae dataset. Figures 14 and 15 display posterior distributions when fitting to these datasets for comparison with Figure 7.

Pearson	$\log(10^{10}A_s)$	n_s	H_0	ω_b	ω_{cdm}	τ_{reio}	w_0	w_a
$\log(10^{10}A_s)$	1.00	0.51	-0.01	0.44	-0.65	0.99	-0.31	0.49
n_s	0.51	1.00	0.00	0.44	-0.67	0.52	-0.26	0.44
H_0	-0.01	0.00	1.00	0.08	0.01	-0.01	-0.53	0.18
ω_b	0.44	0.44	0.08	1.00	-0.52	0.43	-0.20	0.37
ω_{cdm}	-0.65	-0.67	0.01	-0.52	1.00	-0.65	0.39	-0.64
τ_{reio}	0.99	0.52	-0.01	0.43	-0.65	1.00	-0.30	0.48
w_0	-0.31	-0.26	-0.53	-0.20	0.39	-0.30	1.00	-0.90
w_a	0.49	0.44	0.18	0.37	-0.64	0.48	-0.90	1.00

Partial	$\log(10^{10}A_s)$	n_s	H_0	ω_b	ω_{cdm}	τ_{reio}	w_0	w_a
$\log(10^{10}A_s)$	—	-0.10	0.05	0.04	0.06	0.98	0.05	0.06
n_s	-0.10	—	0.05	0.05	-0.12	0.12	0.05	0.05
H_0	0.05	0.05	—	0.76	-0.89	-0.04	-0.99	-0.98
ω_b	0.04	0.05	0.76	—	0.63	-0.03	0.76	0.75
ω_{cdm}	0.06	-0.12	-0.89	0.63	—	-0.08	-0.91	-0.92
τ_{reio}	0.98	0.12	-0.04	-0.03	-0.08	—	-0.05	-0.05
w_0	0.05	0.05	-0.99	0.76	-0.91	-0.05	—	-1.00
w_a	0.06	0.05	-0.98	0.75	-0.92	-0.05	-1.00	—

Table 8: Pearson correlations (top) and partial correlations (bottom) between the cosmological parameters in the w_0w_a CDM model with the dataset **CMB-P(EE)+B+SN_{DES}**.

Pearson	$\log(10^{10}A_s)$	n_s	H_0	ω_b	ω_{cdm}	τ_{reio}	w_0	w_a
$\log(10^{10}A_s)$	1.00	0.51	0.10	0.45	-0.66	0.99	-0.32	0.48
n_s	0.51	1.00	0.09	0.44	-0.67	0.52	-0.28	0.43
H_0	0.10	0.09	1.00	0.14	-0.12	0.10	-0.78	0.53
ω_b	0.45	0.44	0.14	1.00	-0.52	0.43	-0.24	0.37
ω_{cdm}	-0.66	-0.67	-0.12	-0.52	1.00	-0.66	0.41	-0.63
τ_{reio}	0.99	0.52	0.10	0.43	-0.66	1.00	-0.32	0.47
w_0	-0.32	-0.28	-0.78	-0.24	0.41	-0.32	1.00	-0.93
w_a	0.48	0.43	0.53	0.37	-0.63	0.47	-0.93	1.00

Partial	$\log(10^{10}A_s)$	n_s	H_0	ω_b	ω_{cdm}	τ_{reio}	w_0	w_a
$\log(10^{10}A_s)$	—	-0.10	0.03	0.07	0.05	0.98	0.04	0.05
n_s	-0.10	—	0.08	0.03	-0.10	0.13	0.08	0.08
H_0	0.03	0.08	—	0.75	-0.88	-0.03	-0.99	-0.98
ω_b	0.07	0.03	0.75	—	0.61	-0.05	0.75	0.75
ω_{cdm}	0.05	-0.10	-0.88	0.61	—	-0.08	-0.90	-0.91
τ_{reio}	0.98	0.13	-0.03	-0.05	-0.08	—	-0.04	-0.05
w_0	0.04	0.08	-0.99	0.75	-0.90	-0.04	—	-1.00
w_a	0.05	0.08	-0.98	0.75	-0.91	-0.05	-1.00	—

Table 9: Pearson correlations (top) and partial correlations (bottom) between the cosmological parameters in the w_0w_a CDM model with the dataset **CMB-P(EE)+B+SN_{Union3}**.

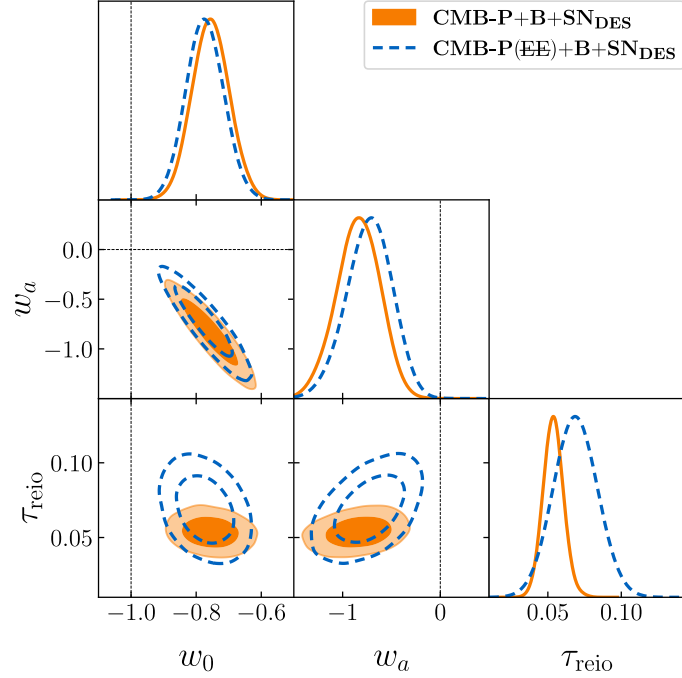


Figure 14: The one- and two-dimensional posterior distributions of τ_{reio} , w_0 , and w_a when fit to **CMB-P+B+SN_{DES}** and **CMB-P(EE)+B+SN_{DES}**.

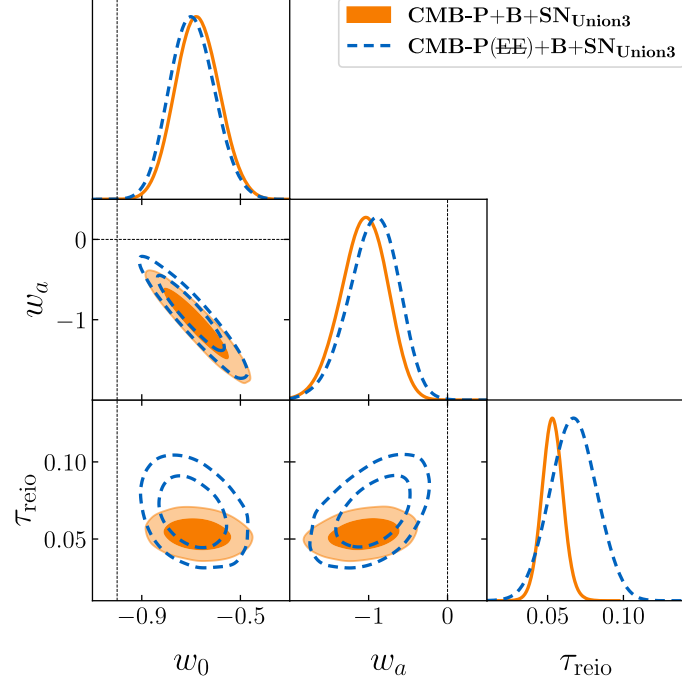


Figure 15: The one- and two-dimensional posterior distributions of τ_{reio} , w_0 , and w_a when fit to **CMB-P+B+SN_{Union3}** and **CMB-P(EE)+B+SN_{Union3}**.

Parameter	CMB-PAS+B+SN	CMB-PAS(EE)+B+SN
$\log(10^{10} A_s)$	$3.065^{+0.012}_{-0.014}$	$3.108^{+0.018}_{-0.018}$
n_s	$0.9737^{+0.0025}_{-0.0025}$	$0.9758^{+0.0026}_{-0.0026}$
ω_{cdm}	$0.11787^{+0.00059}_{-0.00059}$	$0.11725^{+0.00060}_{-0.00059}$
ω_b	$0.022408^{+0.000087}_{-0.000086}$	$0.022442^{+0.000088}_{-0.000088}$
H_0 [km/s/Mpc]	$68.20^{+0.24}_{-0.24}$	$68.46^{+0.25}_{-0.25}$
τ_{reio}	$0.0663^{+0.0066}_{-0.0078}$	$0.092^{+0.010}_{-0.010}$

Table 10: Posterior mean values and corresponding 68% C.L. intervals for the cosmological parameters in the Λ CDM model when fit to **CMB-PAS+B+SN** and **CMB-PAS(EE)+B+SN**.

Parameter	CMB-PAS+B+SN	CMB-PAS(EE)+B+SN
$\log(10^{10} A_s)$	$3.059^{+0.012}_{-0.014}$	$3.108^{+0.021}_{-0.026}$
n_s	$0.9729^{+0.0025}_{-0.0026}$	$0.9756^{+0.0029}_{-0.0029}$
ω_{cdm}	$0.11819^{+0.00059}_{-0.00059}$	$0.11728^{+0.00087}_{-0.00071}$
ω_b	$0.022394^{+0.000089}_{-0.000089}$	$0.022439^{+0.000092}_{-0.000095}$
H_0 [km/s/Mpc]	$68.37^{+0.25}_{-0.26}$	$68.43^{+0.32}_{-0.29}$
τ_{reio}	$0.0631^{+0.0067}_{-0.0076}$	$0.091^{+0.012}_{-0.015}$
$\sum m_\nu$ [eV]	< 0.0613 (95% C.L.)	< 0.142 (95% C.L.)

Table 11: Posterior mean values and corresponding 68% C.L. intervals for the cosmological parameters in the Λ CDM+ $\sum m_\nu$ model when fit to **CMB-PAS+B+SN** and **CMB-PAS(EE)+B+SN**.

D Posteriors for CMB-PAS

The combination **CMB-PAS** combines CMB data from *Planck*, ACT, and SPT, using the highest precision from each dataset to try to get the most constraining power from CMB data. We present posterior statistics and plots from this novel combination in this section. Table 10 gives the 68% C.L. marginalized statistics for Λ CDM parameters fit to the combinations **CMB-PAS+B+SN** and **CMB-PAS(EE)+B+SN**, with the corresponding posterior distributions plotted in Figure 16. In addition, posteriors for Λ CDM+ $\sum m_\nu$ are given in Table 11 and Figure 17.

We obtain a novel upper bound on the total neutrino mass $\sum m_\nu < 0.061$ eV, which is slightly weaker than the bound from the combination of *Planck*, ACT, and SPT implemented by the SPT collaboration in [49] ($\sum m_\nu < 0.048$ eV). This difference is most likely driven by our inclusion of the Pantheon+ supernovae dataset, which is known to increase the bound on $\sum m_\nu$ (see [59, 60]), but it may also be somewhat dependent on our different choices of ℓ -ranges for each CMB dataset compared to the choices made by the SPT collaboration. In addition, the prior on τ_{reio} utilized by the SPT collaboration has also been shown to drive down the constraint a bit, see [31] for more details. Nonetheless, since this upper bound includes all current CMB datasets, the most recent DESI BAO results, and one of three complementary supernovae datasets, it can be considered the most complete and up-to-date constraint on neutrino mass in the Λ CDM+ $\sum m_\nu$ context.

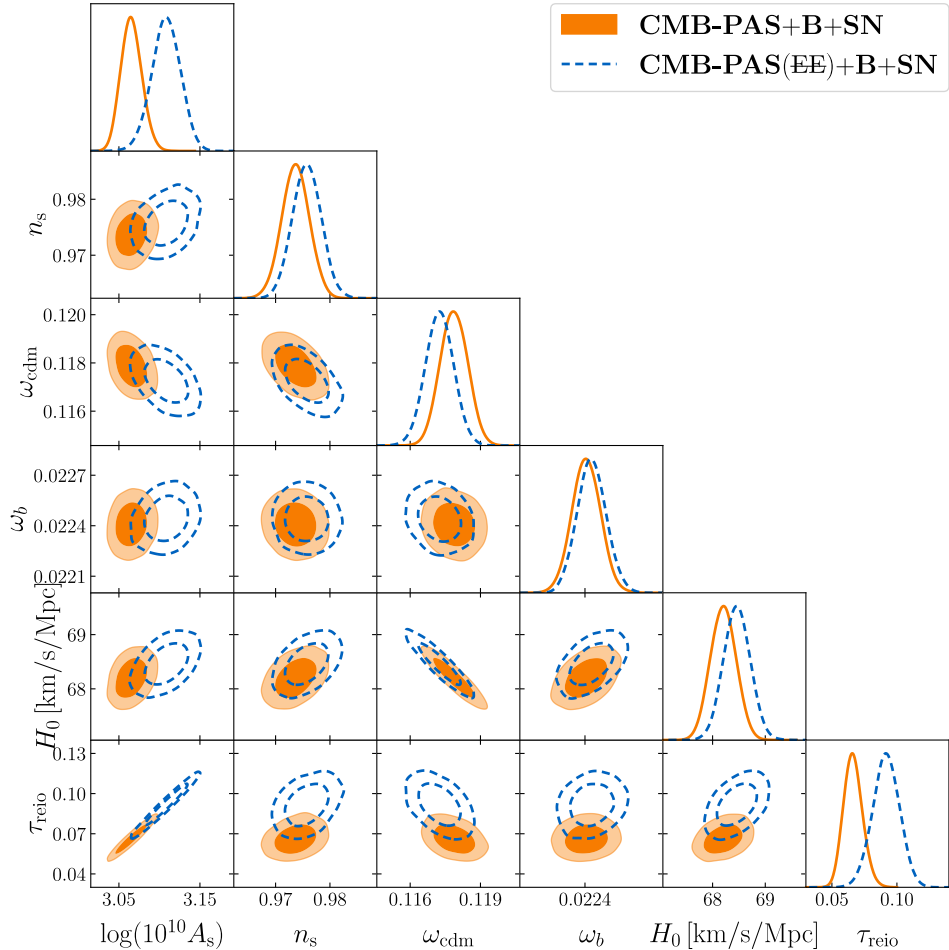


Figure 16: The one- and two-dimensional posterior distributions of all cosmological parameters for the Λ CDM model when fit to **CMB-PAS+B+SN** and **CMB-PAS(EE)+B+SN**.

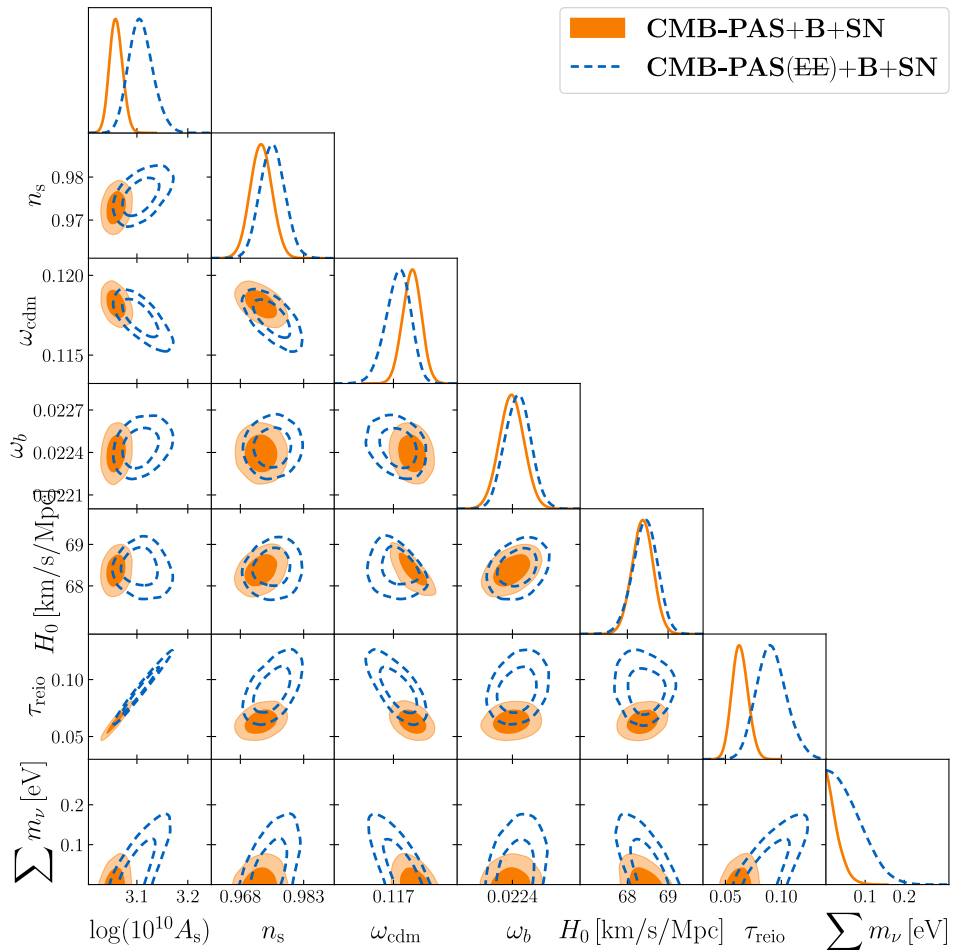


Figure 17: The one- and two-dimensional posterior distributions of all cosmological parameters for the Λ CDM+ $\sum m_\nu$ model when fit to **CMB-PAS+B+SN** and **CMB-PAS(EE)+B+SN**.